Power Waveforming: Wireless Power Transfer Beyond Time Reversal

Meng-Lin Ku, *Member, IEEE*, Yi Han, Hung-Quoc Lai, *Member, IEEE*, Yan Chen, *Senior Member, IEEE*, and K. J. Ray Liu, *Fellow, IEEE*

***Abstract*—This paper explores the idea of time-reversal (TR) technology in wireless power transfer to propose a new wireless power transfer paradigm termed power waveforming (PW), where a transmitter engages in delivering wireless power to an intended receiver by fully utilizing all the available multipaths that serve as virtual antennas. Two power transfer-oriented waveforms, energy waveform and single-tone waveform, are proposed for PW power transfer systems, both of which are no longer TR in essence. The former is designed to maximize the received power, while the latter is a low-complexity alternative with small or even no performance degradation. We theoretically analyze the power transfer gain of the proposed power transfer system over the direct transmission scheme, which can achieve about 6 dB gain, under various channel power delay profiles and show that the PW is an ideal paradigm for wireless power transfer because of its inherent ability to recollect all the power that is possible to harvest from the surrounding environment. In addition, the outage performances in harvesting power of the PW system and the conventional multiple-input multiple-output (MIMO) system are derived. It reveals that the PW system can achieve the same outage performance of the MIMO system as long as the number of resolvable multipaths is sufficiently large. Simulation results validate the analytical findings and experimental results demonstrate the effectiveness of the proposed PW technique.**

***Index Terms*—Wireless power transfer, power waveforming, ultra-wideband, multipath channels.**

I. Introduction

THE advent of Internet of Things (IoT) era is anticipated to facilitate ubiquitous wireless connections of many devices, enabling not only data collection from the surrounding environments but also data exchange and interaction with other devices. Unlike the traditional wireless communications which are primarily limited by the availability of spectrum resource, wireless devices in the future are further subject to an energy-hungry problem due to the explosive growth of wireless data services [1]. In particular, such an embarrassment is unavoidable when wireless devices are untethered to a power grid and can only be supplied by batteries with limited capacity [2]. In order to prolong the network lifetime, one immediate solution is to frequently replace batteries before the battery is exhausted, but unfortunately, this strategy is inconvenient, costly and dangerous for some emerging wireless applications, e.g., sensor networks in monitoring toxic substance.

Recently, energy harvesting has attracted a lot of attention in realizing self-sustainable wireless communications with perpetual power supplies [3], [4]. Being equipped with a rechargeable battery, a wireless device is solely powered by the scavenged energy from the natural environment such as solar, wind, motion, vibration and radio waves. While the ambient energy sources are environmentally friendly, the random, uncontrollable and unpredictable characteristics make it difficult to ensure the quality-of-service (QoS) in wireless communications. For example, the intensity of sunlight is affected by the time of the day, the current weather, the seasonal weather pattern, the surrounding environment, to name but a few [5].

Alternatively, wireless power transfer using electromagnetic radiation has been recognized as an effective and viable technology to provide reliable energy sources for dedicated low-powered wireless devices, e.g., sensors and radio-frequency identification (RFID) [6]. A comprehensive survey of wireless charging technologies, along with the progress in standardization and the recent advances in network applications, has been studied in [7]. The conventional wireless power transfer technologies include electromagnetic induction coupling, magnetic resonant coupling, and radio frequency (RF) signals [8]. The energy transfer efficiency of the first two technologies is higher than 80%, whereas they are only suitable for short-distance energy transfer applications within a distance of a wavelength. On the other hand, electromagnetic radiation which appears in the form of RF signals can propagate up to tens of meters, and the power can be extracted at receive antennas through rectifier circuits; however, the energy transfer efficiency is relatively low due to the severe propagation loss. As compared with the ambient energy sources, the main advantage of wireless power transfer is that a dedicated electromagnetic radiation source is capable of delivering an on-demand energy supply. In this paper, we will focus on the investigation of a RF signal-based power transfer system, since it is expected to play an important role in unplugged wireless applications in the near future.

The design of the RF signal-based power transfer systems faces two essential challenges. First, the required power sensitivity of an energy receiver is much higher than that for an information receiver, e.g., 50 dBm for information receivers and -10 dBm for energy receivers [9]. Second, the power density of wireless signals at receive antennas is degraded by multipath channels, shadowing effect and large-scale path loss, and only a

Manuscript received February 17, 2016; revised June 20, 2016; accepted August 4, 2016. Date of publication August 18, 2016; date of current version September 21, 2016. The associate editor coordinating the review of this paper and approving it for publication was Prof. Tsung-Hui Chang.

M.-L. Ku is with the Department of Communication Engineering, National Central University, Taoyuan 320, Taiwan, and also with Origin Wireless, Inc., Boston, MA 02116 USA (e-mail: mlku@ce.ncu.edu.tw).

Y. Han and K. J. R. Liu are with the Department of Electrical and Computer Engineering, University of Maryland, College Park, MD 20742 USA, and also with Origin Wireless, Inc., Boston, MA 02116 USA (e-mail: yhan1990@umd.edu; kjrliu@umd.edusa).

H.-Q. Lai is with Origin Wireless, Inc., Boston, MA 02116 USA (e-mail: quoc.lai@originwireless.net).

Y. Chen is with the School of Electronic Engineering, University of Electronic Science and Technology of China, Chengdu 610051, China, and also with Origin Wireless, Inc., Boston, MA 02116 USA (e-mail: eecyan@uestc.edu.cn).

Color versions of one or more of the figures in this paper are available online at http://ieeexplore.ieee.org.

Digital Object Identifier 10.1109/TSP.2016.2601283

small fraction of energy emitted from the transmitter can be harvested at the receiver, resulting in an energy scarcity problem. By harnessing spatial degree-of-freedom of multiple antennas, beamforming techniques have been widely applied to combat the severe signal power loss over distance and to enhance the energy transfer efficiency. Specifically, in wireless power transfer, multiple transmit antennas facilitate focusing a sharp energy beam at an intended receiver, while multiple receive antennas enlarge the effective aperture area.

Various energy beamforming schemes have been studied in the literature [10]–[16]. In [10], the authors emphasized the performance enhancement by employing multi-antenna techniques, and a tradeoff between wireless information and power transfer was investigated under two cases: a limited feedback multi-antenna technique and a large-scale multiple-input multiple-output (MIMO) technique. In [11], a new network architecture was proposed to enable mobile recharging, where a cellular system is overlaid with randomly deployed power stations which could radiate power isotropically or directionally toward mobile users by beamforming. In [12], the authors considered wireless powered communications with a multi-antenna access point, where users' data transmission in the uplink fully hinges on the wireless power from the access point in the downlink. The authors in [13] designed energy beamforming for wirelessly charging multiple RFID tags, and both channel-training energy and energy allocation weights were jointly optimized. In [14], a distributed energy beamforming scheme was developed for reaching a compromise between simultaneous wireless information and power transfer in two-way relay channels, and superimposed energy and information-bearing signals were proposed to enhance the achievable sum rate. An MIMO energy transfer system was considered in [15] in Rician fading channels with the joint optimization of channel acquisition and transmit beamforming, while an energy beamforming scheme was investigated in [16] for a multiuser MIMO energy transfer system with one-bit channel feedback. Some existing works applied a massive antenna array for wireless power transfer [17]–[24]. In [17], an outage probability for which the energy harvested by a node is less than the energy spent on uplink pilots was analyzed with a huge number of transmit antennas. The works in [18] and [24] focused on an MIMO system equipped with a large-scale antenna array and examined the impact of the number of antennas on the energy transfer performance.

However, there are two drawbacks when utilizing multiple antennas for wireless power transfer. First, additional RF chains increase the implementation cost. Second, for indoor rich scattering environments, which are the most desired application scenarios for wireless energy transfer, the beamforming schemes may not work appropriately because the line-of-sight (LOS) link may be blocked by impenetrable objects or attenuated by penetration loss.

Motivated by the above discussions, three fundamental and interesting questions are raised: (1) Can/how a wireless power transfer system wirelessly charge a remote device in non-line-of-sight (NLOS) environments? (2) Can/how wireless power transfer be enabled by a low-complexity system, e.g., a single antenna? (3) Can/how the multipath signals, if exists, act as a useful resource for wireless power transfer? Generally speaking, the efficiency of wireless power transfer using omni-directional antennas in the NLOS channels could be very poor because the scatters in the environments will disperse the radiated power to multiple replicas of transmitted signals. In this regard, it is possible to sustain the receiver with a better harvested power level if the power on each multipath can be constructively recollected. While the wireless power transfer has been extensively investigated in the recent literature, the aforementioned questions have not been fully addressed and remain to be answered, and the use of multipaths brings a new research opportunity in designing the wireless power transfer technologies.

Thanks to its ability to making full use of multipath propagation, time-reversal (TR) transmission in a rich-scattering environment has been recognized as an ideal paradigm for low-complexity single-carrier broadband wireless communications [20], [21]. The transmission consists of two phases. During the first phase, a receiver sends an ideal impulse signal to a transmitter for probing the channel impulse response (CIR) of the link. With channel reciprocity, the transmitter simply sends a time-reversed conjugate waveform according to the CIR, which is also called a basic TR waveform, in order to leverage the multipath channel as a cost-free matched filter and to refocus the signal power at the receiver. This phenomenon is commonly referred to as a spatial-temporal focusing effect [22], since it concentrates the signal power at a particular time instant and an intended spatial location. In spite of this focusing advantage, the large delay spread causes severe inter-symbol interference (ISI), thus waste of energy, especially when the data rate is high. To compensate for this vulnerability, a new waveform, referred to as MaxSINR waveform, was designed in [23] to maximize the signal-to-interference plus noise ratio (SINR) at the receiver. However, none of these previous works attempts to design a wireless power transfer system by taking good advantage of multipath propagation to sustain the received power at an energy receiver. Also the performance of such a wireless power transfer system has not been investigated.

In this paper, we propose the new concept of power transfer waveform design generalized from the TR system, called power waveforming (PW), that utilizes all available multipaths as virtual antennas to recollect all power that can be possibly harvested for power transfer, and provide a quantitative performance analysis of the PW power transfer system. Specifically, the novelty and the contributions of this paper are summarized as follows:

- Most of the existing works studied wireless power transfer problems in flat fading channels, e.g., massive MIMO systems in [24], multiple-input single-output (MISO) broadcasting systems in [25], and joint design of training and power transfer in [15]. Some recent works, like [26]–[28], considered orthogonal frequency division multiplexing (OFDM)-based wireless power transfer in frequency selective fading channels. However, the first two designs mainly focus on the optimization of power and sub-band allocation for simultaneous information and wireless power transfer, and the sub-bands are assumed to be independent of each other. The third design also optimizes the net harvested energy over independent sub-bands for MISO systems. To the best of our knowledge, this paper is the first work to comprehensively study the use/impact of multipaths on the wireless power transfer. An optimal energy waveform is proposed for the PW power transfer system to maximize the received power at the receiver side by constructively recollecting the dispersed signal power in the multipath channel.
- We also discover a single-tone waveform which only concentrates its full waveform power on the principle

frequency component with the largest amplitude. As compared with the energy waveform, the single-tone waveform has much lower computational complexity in implementation, whereas it can achieve a comparable (near optimal) power transfer performance. We show that the single-tone waveform is exactly the same as the optimal energy waveform, if the transmitted signal is J-periodic, where J is an integer ratio between the number of multipaths and the backoff factor.

- A rigorous performance analysis for the single-tone waveform is conducted and several quantitative findings are provided. We first define a power transfer gain which is a ratio between the average power transfer performances of the single-tone waveform and the direct transmission, and this gain can serve as a lower bound for the gain of the optimal energy waveform over the direct transmission. A finite-integral expression of the power transfer gain is derived under general power delay profiles. Furthermore, we obtain a closed-form expression for the power transfer gain in uniform power delay profiles (UPD) as well as a performance lower bound in triangular power delay profiles (TPD).
- The outage performances in harvesting power of the proposed PW power transfer system and the conventional MIMO power transfer system with transmit beamforming are theoretically derived. We propose a new notion of power transfer outage to measure the performance of wireless power transfer, which is different from the traditional definition adopted in information decoding. Specifically, a power transfer system is in outage if the harvested power is not larger than a preset threshold. Our analysis shows that the PW system offers great promise in achieving a comparable performance to the MIMO system if the number of resolvable multipaths is sufficiently large. The proposed PW power transfer system, however, only requires a single transmit and receive antenna. For example, a PW system with 6 paths and 24 paths can achieve the same outage probability of 0.9 as an MIMO system with $(N_T, N_R) = (2, 1)$ and $(3, 1)$, respectively, where N_T and N_R are the numbers of transmit and receive antennas.
- Extensive computer simulations are performed to validate the theoretical results in various channel models, including ultra-wideband (UWB) channels in LOS and NLOS office environments, UPD, TPD and exponential decay power delay (EPD) channel profiles, etc. Several waveforms, including direct transmission, energy waveform, single-tone waveform, basic TR waveform and MaxSINR waveform, are simulated for performance comparisons. It is found that the power transfer performance is dependent on the extent of the multipath effect, and the power transfer gain provided by the single-tone waveform over the direct transmission is approximately given by 6 dB under practical multipath conditions. In addition, real experiments are conducted to verify the performance of the proposed waveforms in LOS and NLOS experimental settings in indoor environments, and it is shown that the PW technique can improve the wireless power transfer efficiency by about 400 %$\sim$ 800% (6 dB $\sim$ 9 dB) with a single antenna only, as compared with the direct transmission.

The following notations are used throughout this paper. The uppercase and lowercase boldface letters denote matrices and vectors, respectively. The notations $(\cdot)^T$, $(\cdot)^\dagger$, $(\cdot)^*$ and $(\cdot)^{-1}$ stand for transpose, conjugate transpose, element-wise conjugate and inverse operation, respectively. The matrix $\mathbf{I}_N$ represents an $N \times N$ identity matrix. The notations $\mathbb{E}[\cdot]$ and $\|\mathbf{x}\|_2$ take expectation and the Euclidean norm of a vector $\mathbf{x}$. The operator $\max(x, y)$ takes the maximum value between x and y, while the operator $\min(x, y)$ finds the minimum value.

The rest of this paper is organized as follows. In Section II, we introduce the system model for the PW systems, generalized from the TR systems, with multipath channels. Two power transfer waveforms are presented in Section III. Section IV is devoted to analyze the power transfer gain under different channel power delay profiles. The outage performances of the PW system and the conventional MIMO system are analyzed and compared in Section V. Simulation and numerical results are presented in Section VI, and experimental results are given in Section VII. Finally, conclusions are drawn in Section VII.

II. System Model

In this paper, we consider an L-tap wireless fading channel, and the channel is assumed to be quasi-static over the observation time. The CIR between the transmitter and the receiver can be modeled as

$$h[n] = \sum_{l=0}^{L-1} h_l \delta[n-l], \quad n = 0, \ldots, L-1, \tag{1}$$

where $\delta[n]$ is the Kronecker delta function, and h_l is the channel gain of the l^{th} path, which is a circularly symmetric complex Gaussian random variable with zero mean and variance $\mathbb{E}[|h_l|^2] = \rho_l$, for $l = 0, \ldots, L-1$. Without loss of generality, we assume that the total channel power is one, i.e., $\sum_{l=0}^{L-1} \rho_l = 1$. For simplicity, it is further assumed that the paths of CIR are uncorrelated with each other, i.e., $\mathbb{E}[h_i h_j^*] = 0$, for $i \neq j$. Besides, the in-phase and quadrature components of each path are also uncorrelated with each other and contain identical power. Note that in practice, the number of resolvable paths increases as the system bandwidth becomes wider, and the number of resolvable paths will reach a limit when the system bandwidth is sufficiently large, which is the maximal number of resolvable paths in the wireless environments.

We first review the signal processing procedures in the TR systems, where a focusing effect is created at the intended receiver by exploiting the multipath propagation to recollect all the possibly available path energy from the wireless environment [20]. To achieve this, the receiver first sends a pilot signal with a delta-like auto-correlation function to measure the CIR at the transmitter side during a channel probing phase. With the channel reciprocity assumption, the transmitter then forms a waveform $g[n]$ to send data symbols according to the channel state information (CSI). Typically, the baud rate is much lower than the sampling rate. Let $\{v_D[n]\}_{n=0}^{(N-1)D}$ be the up-sampling signal of data symbols $\{v[n]\}_{n=0}^{N-1}$, where N is the number of total transmitted data symbols, given by

$$v_D[n] = \begin{cases} v[n/D], & n \bmod D = 0; \\ 0, & \text{otherwise}, \end{cases} \tag{2}$$

where D is a rate back-off factor, which is a ratio of the sampling rate and the baud rate, and $\mathbb{E}[|v[n]|^2] = P$. Hence, the transmitted signal $\{s[n]\}_{n=0}^{L-1+(N-1)D}$ after waveform mapping

can be expressed as[‖]

$$s[n] = (v_D * g)[n]. \tag{3}$$

Furthermore, the signal received at the receiver, $\{y_D[n]\}_{n=0}^{2L-2+(N-1)D}$, is given as

$$\begin{aligned} y_D[n] &= (h * s)[n] + z[n] = (f * v_D)[n] + z[n] \\ &= \sum_{l=0}^{2L-2} f[l]\, v_D[n-l] + z[n], \end{aligned} \tag{4}$$

where $f[n] = (h * g)[n]$ is defined as an equivalent impulse response, for $n = 0, \ldots, 2L-2$, and $z[n]$ is additive complex white Gaussian noise with zero mean and variance σ_z^2. A basic TR waveform is a time reversed conjugate version of the CIR, given as [20]

$$g_{TR}[n] = \frac{h^*[L-1-n]}{\sqrt{\sum_{l=0}^{L-1} |h[n]|^2}}, \quad n = 0, \ldots, L-1. \tag{5}$$

From (4), it is found that the wireless channel naturally performs the operation of matched filtering with respect to $g_{TR}[n]$, and a peak is observed in the received signal $y_D[n]$ for data detection. To further suppress the ISI, a waveform, $g_{\mathrm{SINR}}[n]$, is designed in [23] to maximize the SINR. It is also worth mentioning that if there is no particular design for the waveform, i.e., $g_{DT}[n] = \delta[n]$, the considered system model is degenerated to the conventional direct transmission scheme. The waveforms $g_{TR}[n]$, $g_{\mathrm{SINR}}[n]$ and $g_{DT}[n]$, however, are not eligible for power transfer, since they are mainly designed from the perspective of information transfer and the ISI due to the multipath effect is not appropriately utilized as a green source of energy. The PW power transfer system follows the same signal processing procedures and models presented in (2)–(4), but new waveforms are designed for the purpose of wireless power transfer and $v[n]$ is defined as a non-information-bearing sequence. For simplicity, we assume that this sequence is random in order to evaluate the wireless power transfer performance in an average sense over distinct random sequences. In the following section, we aim at finding the power transfer waveforms for the PW systems.

III. Power Transfer Waveform Designs

A. Optimal Energy Waveform

By substituting (2) into (4) and applying change of variables, it yields

$$\begin{aligned} y_D[n] &= \sum_{l=\lceil (n-2L+2)/D \rceil}^{\lfloor n/D \rfloor} f[n-lD]\, v[l] + z[n] \\ &= \sum_{l=\lceil (n-2L+2)/D \rceil}^{\lfloor n/D \rfloor} \sum_{m=0}^{L-1} g[m]\, h[n-lD-m] v[l] + z[n], \end{aligned} \tag{6}$$

where $\lceil \cdot \rceil$ and $\lfloor \cdot \rfloor$ are the ceiling and floor functions, respectively. Our design goal is to find an optimal energy waveform to maximize the average power transferred to the receiver side, given by

$$\begin{aligned} \mathbf{g}_E = \arg \max_{\|\mathbf{g}\|_2^2 = 1} \Bigg(& \lim_{N \to \infty} \frac{1}{2L-1+(N-1)D} \\ & \cdot \sum_{n=0}^{2L-2+(N-1)D} \mathbb{E}\left[|y_D[n]|^2 \right] \Bigg), \end{aligned} \tag{7}$$

where $\mathbf{g} = [g[0], \ldots, g[L-1]]^T$ is the waveform vector. Let $\mathbf{y}_p = [y_D[L-1+(p-1)D+1], \ldots, y_D[L-1+pD]]^T$ be the p^{th} segment of the received signal $y_D[n]$, and $\mathbf{H}$ be a $(2L-1) \times L$ Toeplitz channel matrix with the column vector $[h[0], \ldots, h[L-1], 0, \ldots, 0]^T$ as its first column. We can rewrite (6) in a compact matrix form as follows:

$$\mathbf{y}_p = \sum_{q=\lceil p-1-(L-2)/D \rceil}^{\lfloor p+(L-1)/D \rfloor} \mathbf{H}_{(q-p)} \mathbf{g} \cdot v[q] + \mathbf{z}_p, \tag{8}$$

where $\mathbf{z}_p$ represents the noise term contained in the p^{th} segment, and the matrix $\mathbf{H}_j$ is defined as

$$\mathbf{H}_j = \left[\mathbf{O}_{(a_l - L + (j+1)D) \times L}^T, \mathbf{B}^T, \mathbf{O}_{(L-1-jD-a_u) \times L}^T \right]^T, \tag{9}$$

where $a_l = \max(0, (L-(j+1)D))$, $a_u = \min(2L-2, (L-1-jD))$, and $\mathbf{B}$ is a submatrix of the Toeplitz channel matrix $\mathbf{H}$, containing the entries from the a_l^{th} row to the a_u^{th} row of $\mathbf{H}$. Without loss of generality, we assume that the number of channel taps is finite, and the time duration of the transmitted signals is sufficiently larger, i.e., $N \gg L$. From (7), as N goes to infinity, the average power transfer maximization problem is equivalent to maximizing the sum power of the p^{th} segment:

$$\mathbf{g}_E = \arg \max_{\|\mathbf{g}\|_2^2 = 1} \mathbb{E}\left[\|\mathbf{y}_p\|_2^2 \right], \tag{10}$$

where the total power of the designed waveform is subject to one.

Theorem 1: If the signals $v[n]$ are uncorrelated, i.e., $\mathbb{E}[v[i]\, v^*[j]] = 0, \forall i \neq j$, the optimal energy waveform is given by

$$\mathbf{g}_E = \mathbf{u}_1, \tag{11}$$

where $\mathbf{u}_1$ is the principal eigenvector of the matrix $\sum_{q=\lceil -1-(L-2)/D \rceil}^{\lfloor (L-1)/D \rfloor} \mathbf{H}_q^\dagger \mathbf{H}_q$.

Proof: The proof is provided in Appendix A. ■

An example of the optimal energy waveform for UWB channels is demonstrated in Fig. 1 under NLOS environments [29]. Fig. 1(a) shows the amplitude of the CIR as well as the corresponding channel frequency response (CFR). Fig. 1(b) sketches the amplitude of the optimal energy waveform and its frequency response, which is the discrete Fourier transform (DFT) of the time-domain waveform $\mathbf{g}_E$. A closer look at this figure reveals that the energy waveform tends to concentrate its waveform power on those frequency components ($k = 9$, 10, and 11) with the largest amplitude of the CFR. Interestingly, each tap of the optimal energy waveform has comparable gain in order to spread out the energy of the transmitted signals over the entire time duration, which is different from other waveform designs as depicted in Fig. 2.

[‖]The PW schemes are implemented digitally. Before it is radiated, the discrete-time signal is converted into a continuous-time signal with common signal processing at the transmitter, e.g., pulse-shaping filters, digital-to-analog converters, up-converters. For simplicity, equivalent baseband representation is considered here.

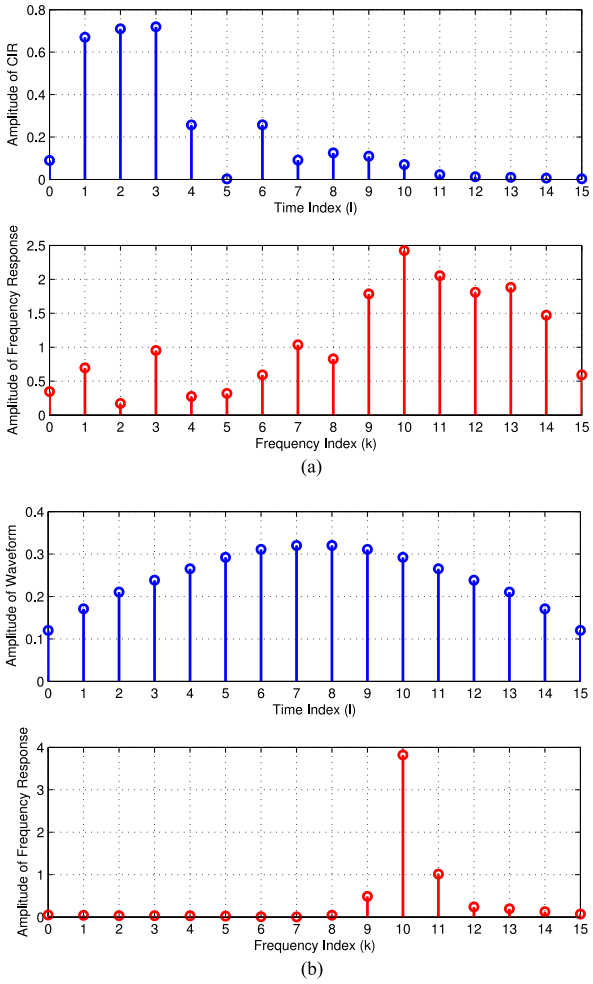

Fig. 1. An example of the optimal energy waveform for UWB channels in NLOS office environments. (a) UWB channels. (b) Optimal energy waveform.

B. Single-Tone Waveform

Define $\mathbf{F}$ as a DFT matrix, whose $(m,n)^{th}$ entry is given by $\frac{1}{\sqrt{L}}e^{-j2\pi mn/L}$, for $m,n=0,\ldots,L-1$, and the CFR of the CIR $\mathbf{h}=[h[0],\ldots,h[L-1]]^T$ can be calculated as $\boldsymbol{\zeta}=\mathbf{Fh}=[H[0],\ldots,H[L-1]]^T$. Motivated by the observation in Fig. 1, a single-tone waveform $\mathbf{g}_{ST}=[g_{ST}[0],\ldots,g_{ST}[L-1]]^T$ is proposed as follows:

$$g_{ST}[n]=\frac{1}{\sqrt{L}}e^{-j\frac{2\pi k_{\max}n}{L}},\quad n=0,\ldots,L-1, \tag{12}$$

where $k_{\max}=\arg\max_k |H[k]|^2$ denotes the principal frequency component. Remember that the optimal energy waveform is designed by maximizing the average received power in time domain; hence, it is superior to any other waveforms, and the harvested power with the single-tone waveform can serve as a performance lower bound for the maximum received power that can be achieved by the optimal energy waveform. In the following, we provide a theorem to link the relationship between the simple single-tone waveform and the optimal energy waveform.

Theorem 2: Assume $L=J\cdot D$, where J is a positive integer number. If the signal $v[n]$ is periodic with the period J, the single-tone waveform is the optimal energy waveform for (10).

Proof: The proof is provided in Appendix B. ■

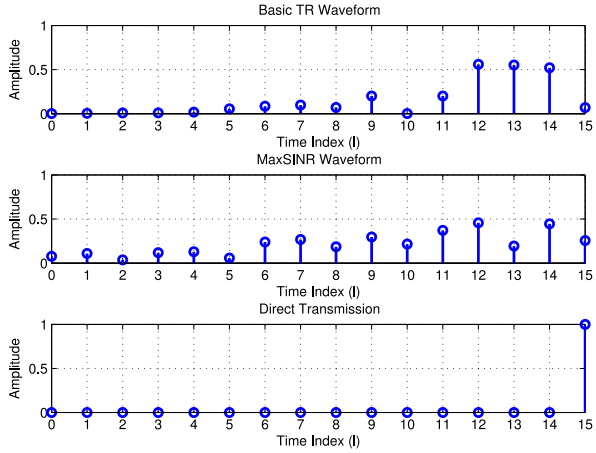

Fig. 2. An example of different waveform designs, including basic TR waveform, MaxSINR waveform, and direct transmission, for UWB channels in NLOS office environments.

TABLE I
COMPLEXITY RATIO BETWEEN OPTIMAL ENERGY AND SINGLE-TONE WAVEFORMS ($D=1$)

L	5	10	15	20	25	30	35
Complexity ratio	32	90	173	278	404	550	716

Since the waveform has a finite length, the single-tone waveform is not the optimal for achieving the maximum average received power if the signal $v[n]$ is not periodic. The above theorem provides a condition for the single-tone waveform to achieve the maximum power transfer value at the receiver. The intuition behind this theorem can be explained as follows. When the transmitted signal is J-periodic, the convolution relation among the transmitted signal $v[n]$, the wireless channel $h[n]$ and the waveform $g[n]$ in (6) becomes the circular convolution; hence, the optimal design of the waveform is to concentrate the total waveform power on the frequency component with the largest amplitude gain in the frequency domain. In general cases, the energy waveform is the optimal design for wireless power transfer, whereas the simulation results in Section VI will demonstrate that the single-tone waveform is near optimal with a minor performance loss. When it comes to the implementation cost, one can find from (11) and (12) that the single-tone waveform has an advantage of low computational complexity over the energy waveform. We evaluate the complexity of the two waveforms in terms of the required number of complex multiplications. To be explicit, the calculation of the energy waveform in (11) involves a sum of matrix-matrix products and a principal eigenvector of a matrix, leading to a complexity of $L^3+(\lfloor\frac{L-1}{D}\rfloor-\lceil-1-\frac{L-2}{D}\rceil+1)DL^2$. On the other hand, the single-tone waveform in (12) requires a DFT and element-wise products to select the main frequency component of the CFR, having a complexity of $L\log_2 L+L$. Taking $D=1$ as an example, the complexity ratio between the energy waveform and the single-tone waveform is approximately given by $\frac{3L^2}{\log_2 L}$ when $L\gg 1$, and some numerical results for different values of L are listed in Table I.

IV. PERFORMANCE ANALYSIS

Since the performance analysis of the optimal energy waveform is almost intractable, we alternatively analyze the power

transfer gain of the proposed single-tone scheme in PW systems as compared with the direct transmission scheme. With loss of generality, we focus on the scenario when the transmitted signals is J-periodic because the single-tone waveform in this case can deliver the maximum received power at the receiver side as the optimal energy waveform. By doing so, the analysis result can help us capture the fundamental limit of the power transfer in multipath environments.

From (B.1)–(B.3), for a given multipath channel, the average power transfer for the single-tone waveform $\mathbf{g}_{ST}$ at the receiver side can be expressed as

$$P_{ST} = \mathbb{E}\left[\|\mathbf{y}_p\|_2^2\right] = P \cdot \mathbf{g}_{ST}^{\dagger}\mathbf{C}^{\dagger}\mathbf{C}\mathbf{g}_{ST}. \tag{13}$$

Here we ignore the noise term in performance analysis, since the noise power is commonly much smaller than the desired received power[¶]. By substituting $\mathbf{g}_{ST} = \mathbf{F}^{\dagger}\mathbf{e}_{k_{\max}}$ into P_{ST} and applying the property $\mathbf{F}\mathbf{C}\mathbf{F}^{\dagger} = \sqrt{L}\cdot\mathrm{Diag}(\boldsymbol{\zeta})$, we get

$$P_{ST} = P\mathbf{e}_{k_{\max}}^{\dagger}\mathbf{F}\mathbf{C}^{\dagger}\mathbf{C}\mathbf{F}^{\dagger}\mathbf{e}_{k_{\max}} = P\cdot L|H\left[k_{\max}\right]|^2. \tag{14}$$

On the other hand, since the direct transmission waveform is expressed as $\mathbf{g}_{DT} = \mathbf{e}_0$, the power transfer performance of the direct transmission scheme for a given channel, $P_{DT} = P\cdot\mathbf{g}_{DT}^{\dagger}\mathbf{C}^{\dagger}\mathbf{C}\mathbf{g}_{DT}$, can be expanded as

$$P_{DT} = P\mathbf{e}_0^{\dagger}\mathbf{F}^{\dagger}\mathbf{F}\mathbf{C}^{\dagger}\mathbf{C}\mathbf{F}^{\dagger}\mathbf{F}\mathbf{e}_0 = P\cdot\sum_{k=0}^{L-1}|H[k]|^2. \tag{15}$$

Definition 1: The power transfer gain G is a ratio between the average power transfer of the single-tone waveform and that of the direct transmission scheme in wireless channels, i.e., $G = \mathbb{E}[P_{ST}]/\mathbb{E}[P_{DT}]$.

Specifically, from (14) and (15), it leads to

$$G = L\cdot\mathbb{E}\left[|H\left[k_{\max}\right]|^2\right], \tag{16}$$

where $\mathbb{E}[\sum_{k=0}^{L-1}|H[k]|^2] = \sum_{l=0}^{L-1}\rho_l = 1$ according to (1). Therefore, it is found that the power transfer gain depends on the frequency selection diversity gain over the correlated multivariate Rayleigh random variables $\varepsilon_k = |H[k]|^2$, for $k = 0,\ldots,L-1$. Intuitively, a larger power transfer gain can be obtained, if the multipath channel is more frequency selective.

Before we begin the performance analysis of the exact power transfer gain, the following theorem regarding the characteristic function of the multivariate random variables ε_k under a given channel power delay profile is first provided.

Theorem 3: Let $\boldsymbol{\omega} = [\omega_0,\ldots,\omega_{L-1}]^T$. For a multipath channel with the power delay profile $\boldsymbol{\rho} = [\rho_0,\ldots,\rho_{L-1}]^T$ in (1), the characteristic function of $\boldsymbol{\varepsilon} = [\varepsilon_0,\ldots,\varepsilon_{L-1}]^T$ is

$$\Psi_{\boldsymbol{\varepsilon}}(j\boldsymbol{\omega}) = \frac{1}{\det\left(\mathbf{I}_L - 2j\cdot\mathrm{Diag}\left(\boldsymbol{\omega}\right)\boldsymbol{\Sigma}\right)}, \tag{17}$$

where $j = \sqrt{-1}$, $\boldsymbol{\Sigma} = \mathbf{F}^{-1}\mathrm{Diag}(\lambda)\mathbf{F}$, $\lambda = [\lambda_0,\ldots,\lambda_{L-1}]^T$, $\lambda_l = \frac{1}{4}(\rho_l + \rho_{((L-l)\%L)})$, for $l = 0,\ldots,L-1$, and the notation $(y\%L)$ takes the modulo operation over y with respect to L.

Proof: The proof is provided in Appendix C. ■

[¶] In practice, the power sensitivity of an energy harvesting receiver is required to be larger than -10 dBm for efficient RF-DC conversion [4]. Hence, the received signal strength for wireless power transfer must be much higher than the noise power level, e.g., -94 dBm for a bandwidth of 100 MHz.

With Theorem 3, a finite-integral expression for the power transfer gain is theoretically derived in the following theorem.

Theorem 4: For a multipath channel with the power delay profile $\boldsymbol{\rho} = [\rho_0,\ldots,\rho_{L-1}]^T$, the power transfer gain G is

$$G = L\int_0^{\infty}\Big(1 - \frac{1}{(2\pi)^L}\int_{-\infty}^{\infty}\cdots\int_{-\infty}^{\infty}\Psi_{\boldsymbol{\varepsilon}}(j\boldsymbol{\omega}) \times\prod_{l=0}^{L-1}\left(\frac{1-e^{-j\omega_l x}}{j\omega_l}\right)d\omega_0\cdots d\omega_{L-1}\Big)dx. \tag{18}$$

Proof: The proof is provided in Appendix D. ■

While the power transfer gain G is analyzed in Theorem 4, it is difficult to analytically express the power transfer gain in a closed-form for general power delay profiles as the involved multiple integrals prohibit further simplification. Instead, to get more insight into the effect of the parameters in power delay profiles, e.g., the number of multipaths, on the power transfer gain while keeping the analysis analytically tractable, we consider two power delay profiles: an UPD profile and a TPD profile, which are defined in the following.

Definition 2: A power delay profile is called UPD with L channel paths, if $\rho_l = \frac{1}{L}$, for $l = 0,\ldots,L-1$.

Definition 3: A power delay profile is called TPD with L channel paths, if $\rho_l = \frac{2(1-L\rho_0)}{(L-1)L}l + \rho_0$, for $l = 0,\ldots,L-1$, where $\frac{1}{L}\le\rho_0\le\frac{2}{L}$.

Notice that in Definition 3, the TPD channel profile is derived under the assumption that the channel path power is linearly decayed with respect to the path delay. When the path power ρ_0 and the number of multipaths L are specified, the TPD profile can be determined with the unity constraint of the total channel power, i.e., $\sum_{l=0}^{L-1}\rho_l = 1$. Although the EPD profile is a common channel model in studying the performance, it is worth mentioning that the TPD profile could be a good approximation for the EPD profile, especially when the tails of the profile are insignificant. Hence, the TPD profile could be a good alternative to the investigation of the inherent power transfer gain in wireless channels owing to the difficulty in performance analysis by exploiting the EPD profile.

Theorem 5: In a wireless channel with the UPD channel profile, the power transfer gain G is

$$G(L) = \sum_{n=1}^{L}\frac{1}{n}. \tag{19}$$

Proof: The proof is provided in Appendix E. ■

This theorem gives two immediate remarks in the following.

Remark 1: If $L = 1$, the power transfer gain $G(1) = 1$.

In other words, both the direct transmission scheme and the PW system with the single-tone waveform have the same power transfer performance if there is only one LOS path in the wireless environments between the transmitter and the receiver.

Remark 2: In the UPD channel profile, the power transfer gain $G(L)$ is monotonically non-decreasing with the number of multipaths L. Moreover, when the number of multipaths is increased from $L-1$ to L, the gap of $G(L) - G(L-1)$ is given by $\frac{1}{L}$.

From this remark, we can make three important observations for understanding the interaction between the power transfer gain and the number of multipaths. First, the power transfer gain is monotonically increasing with the number of multipaths. From the system point of view, the larger value of L means that

either the bandwidth is wider or the environment becomes more scattering. Second, the improvement on the power transfer gain becomes gradually small as the number of resolvable channel paths is enlarged. Third, the result is analogous to the signal-to-noise power ratio (SNR) increase in the selection combining diversity scheme of a single-input multiple-output (SIMO) system when the number of the receive antennas is increased by one [33]. This is because the single-tone waveform design in the PW system has a similar mathematical model to an SIMO system with antenna selection.

Now we turn to the performance analysis of the power transfer gain in wireless channels with the TPD channel profile. Since it is very tough to deal with the multiple integrals in this case, a performance lower bound is offered in the following theorem.

Theorem 6: In a wireless channel with the TPD channel profile, the power transfer gain G for $L \geq 2$ is lower bounded by[‡]

$$G \geq \frac{L\rho_0 - 1}{L-1} + \frac{L\left(1-\rho_0\right)}{L-1} \sum_{n=1}^{L} \binom{L}{n} (-1)^{n+1} \frac{1}{n}. \quad (20)$$

Proof: The proof is provided in Appendix F. ■

We can further simplify the lower bound formula by substituting $\rho_0 = \frac{a}{L}$, for $1 \leq a \leq 2$, into (20), yielding

$$G\left(L\right) \geq 1 + \frac{L-a}{L-1} \sum_{n=2}^{L} \frac{1}{n}. \quad (21)$$

Remember that the parameter a reflects the decline rate of the TPD channel profile which becomes flatter as the value of a is closer to one. Some interesting remarks are then summarized here. First, for a fixed number of multipaths L, the smaller the value of a is, the larger the lower bound is obtained. Second, for a fixed value of a, the lower bound is monotonically increased with the number of multipaths, since the function $\frac{L-a}{L-1}$ in (21) is an increasing function of L, for $1 \leq a \leq 2$. Third, the lower bound is tight when $a = 1$ or $L = a = 2$ or $L \to \infty$. The first case is because the TPD profile is degenerated to the UPD profile. For the second case, the TPD profile is degenerated to a single-path channel according to Definition 3, i.e., $\rho_0 = 1$ and $\rho_1 = 0$, and thus $G(2) = 1$. The third case can be verified from the proof in Appendix F that the variance of $h_{0,2}$ approaches to zero when $L \to \infty$.

V. Comparisons Between PW Systems and MIMO Systems

In this section, we study the outage performances of the power transfer for the PW systems and the conventional MIMO systems as well as their performance comparisons. It is addressed that the definition of the outage probability is different from the traditional definition used for evaluating the information transfer performance, e.g., SINR and sum rate. The considered outage probability is defined in the following.

Definition 4: A power transfer system is said to be in outage if the harvesting power P_{EH} is smaller than or equal to a preset threshold x, and the outage probability in harvesting power is given as $\Pr(P_{EH} \leq x)$.

First, an $N_T \times N_R$ MIMO system model is introduced, where N_T and N_R are the numbers of transmit and receive antennas, respectively. We assume that the CSI is perfectly available at the transmitter side, and a transmit beamforming technique is applied for wireless power transfer. Hence, the received signal at the receiver can be expressed as

$$\tilde{\mathbf{y}} = \tilde{\mathbf{H}}\tilde{\mathbf{g}}v + \mathbf{z}, \quad (22)$$

where v is the transmitted signal with the power value P, i.e., $\mathbb{E}[|v|^2] = P$, $\tilde{\mathbf{g}}$ is the beamforming vector, $\tilde{\mathbf{H}}$ is an $N_R \times N_T$ identically, independently distributed (i.i.d.) MIMO channel matrix, each entry of which is assumed to be a zero-mean complex Gaussian random variable with the variance one for a fair comparison. Besides, the norm of the beamforming vector is subject to one, i.e., $\|\tilde{\mathbf{g}}\|_2 = 1$. By ignoring the noise term which accounts for an insignificant amount of the entire received signals in reality, the received power is given by $\mathbb{E}[\tilde{\mathbf{y}}^\dagger\tilde{\mathbf{y}}] = P \cdot \tilde{\mathbf{g}}^\dagger\tilde{\mathbf{H}}^\dagger\tilde{\mathbf{H}}\tilde{\mathbf{g}}$. The power transfer can be maximized by choosing the principal eigenvector of the matrix $\tilde{\mathbf{H}}^\dagger\tilde{\mathbf{H}}$, and the power transfer performance for a given channel is computed as

$$P_{\mathrm{MIMO}} = P \cdot \lambda_{\max}\left(\mathbf{H}^\dagger\mathbf{H}\right) = P \cdot \lambda_{\max}\left(\mathbf{H}\mathbf{H}^\dagger\right), \quad (23)$$

where $\lambda_{\max}(\cdot)$ represents the maximum eigenvalue. Notice that the matrix $\mathbf{H}\mathbf{H}^\dagger$ is of the complex Wishart distribution. By directly applying Corollary 2 in [34], the outage probability of the MIMO power transfer can be derived as (24) at the bottom of the page, where $\Gamma(\cdot)$ is the gamma function, $\mathbf{B}(x)$ is a matrix, whose $(i,j)^{th}$ element is given by $\gamma(\max(N_T,N_R) - \min(N_T,N_R) + i + j + 1, \frac{x}{P})$, for $i,\ j = 0, 1, \ldots, \min(N_T,N_R) - 1$, and $\gamma(\cdot,\cdot)$ is the lower incomplete gamma function as specified in [35].

From (D.3) and (E.3), it is known that $F_{\varepsilon_{\max}}(x) = \Pr(|H[k_{\max}]|^2 \leq x) = (1 - e^{-Lx})^L$ when the UPD channel profile is considered. Using (14), we then obtain the outage performance of the single-tone waveform under the UPD channel profile:

$$\Pr(P_{ST} \leq x) = (1 - e^{-x/P})^L. \quad (25)$$

It is interesting to compare the outage performances of the PW system and the conventional MIMO system under the same transmit power value P, and examine how many multipaths are necessary for the PW system to achieve a comparable outage performance as that provided by the MIMO system[§]. In this aspect, we give the following definition:

Definition 5: A PW power transfer system with $L^\star$ resolvable paths is comparable to an $N_T \times N_R$ MIMO power transfer system at an outage probability $\Pr(P_{\mathrm{MIMO}} \leq x) = P_{\mathrm{out}}$, if $L^\star$ is the smallest positive integer which satisfies $\Pr(P_{ST} \leq x) \leq P_{\mathrm{out}}$.

[‡] For the case of $L = 1$, the power transfer gain is equal to one.

[§] The PW and MIMO schemes could be jointly adopted to further boost the system performance by reaping both beamforming and frequency diversity gains.

$$\Pr\left(P_{\mathrm{MIMO}} \leq x\right) = \frac{\det\left(\mathbf{B}(x)\right)}{\prod_{k=1}^{\min(N_T,N_R)} \Gamma\left(\max\left(N_T,N_R\right) - k + 1\right) \cdot \Gamma\left(\min\left(N_T,N_R\right) - k + 1\right)} \quad (24)$$

By using the derived outage probabilities in (24) and (25), it can be shown that the condition $\Pr(P_{ST} \leq x) \leq \Pr(P_{\mathrm{MIMO}} \leq x)$ yields

$$L \geq \frac{1}{\log(1-e^{-x/P})}\Big(\log\det\left(\mathrm{B}(x)\right) - \sum_{k=1}^{\min(N_T,N_R)} \log\left(\Gamma\left(\max\left(N_T,N_R\right)-k+1\right)\right) - \sum_{k=1}^{\min(N_T,N_R)} \log\left(\Gamma\left(\min\left(N_T,N_R\right)-k+1\right)\right)\Big). \quad (26)$$

For a PW power transfer system to achieve the same outage probability of an MIMO power transfer system, the required number of resolvable paths $L^{\star}$ must be equal to the smallest integer not less than the value on the right-hand side of (26).

VI. Simulation Results and Discussions

In this section, we present the performances of the PW wireless power transfer with different designed waveforms, including the energy, single-tone, direct transmission, basic TR and MaxSINR waveforms, by computer simulation, and justify the theoretical findings in Sections IV and V. The system bandwidth is set as 125 MHz, i.e., the sampling period $T_S = 8$ ns. Here, a large bandwidth is required to digitally resolve the naturally existing multipaths for the systems, on which the PW is designed in the digital domain. In other words, without a large bandwidth, the equivalent CIR to the system is likely to be a single tap even though a lot of multipaths exist. However, our finding shows that the optimal energy or single-tone waveforms selectively concentrate the waveform power over a few couple of frequency components or a single frequency component. In practice, the PW system could be possibly operated on a selective portion of the industrial, scientific and medical (ISM) bands on which the proposed waveform concentrates its power, and the remaining bandwidth could be reserved for conventional wireless information transmission. The rate back-off factor D is chosen to be one. The transmitted signal $v[l]$ is assumed to be random and aperiodic and the SNR value is 15 dB, unless otherwise stated. In addition to the UPD and TPD channel profiles, an EPD channel profile is also included in the simulation:

$$\rho_l = c_\rho \cdot e^{-\frac{lT_S}{\sigma_T}}, \quad l = 0, \ldots, L-1, \quad (27)$$

where σ_T is the delay spread of the channel, and c_ρ is a constant such that the summation of ρ_l for all l is equal to one. In a typical indoor environment, the delay spread is on the order of hundreds of nanoseconds, and the total number of resolvable multipaths is around several dozens with respect to $T_S = 8$ ns. If the sampling rate is increased, we could possibly resolve more multipaths, but it is eventually limited by naturally existing multipaths in wireless environments. In the simulation, the average transmit power and the average channel power of different profiles are assumed to be one, i.e., $P = 1$ and $\sum_{l=0}^{L-1} \rho_l = 1$, and we normalize the large-scale path loss effect as our focus is to examine the impact of multipaths on the performance of different waveforms. Accordingly, the average received signal power of the direct transmission scheme is a constant value, given by 0 dB if the noise is excluded, over the number of multipaths. Besides, we simulate the system performance in a Saleh-Valenzuela (SV) channel model [29]. This model is popularly adopted in IEEE 802.15.4a standard and suitable for the wideband applications with a frequency range from 2 to 6 GHz, covering indoor residential, office, outdoor, industrial, and open outdoor environments.

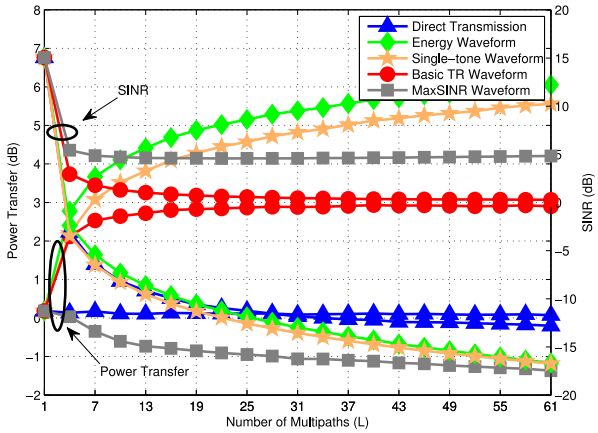

Fig. 3. Power transfer and SINR performances versus number of multipaths under the EPD channel profiles for different waveforms.

Fig. 3 shows the power transfer performance versus the number of multipaths for different waveforms under the EPD channel profiles, along with the corresponding SINR. The delay spread σ_T is set to 160 ns. We can observe that the power transfer performance is monotonically increasing with the number of resolvable paths, except for the direct transmission and the MaxSINR waveforms. Actually, the power transfer performance of the direct transmission keeps constant, while that of the MaxSINR waveform is degraded as L increases. For $L = 61$, the energy waveform and the basic TR waveform outperform the direct transmission by about 6 dB and 3 dB, respectively. Moreover, the energy waveform is superior to the basic TR waveform with a performance gap of 3 dB at $L = 61$. As compared with the energy waveform, the single-tone waveform only incurs a slight performance degradation of no more than 0.5 dB. No matter what waveforms are applied, the SINR performance is degraded as the number of multipaths is increased since the resultant ISI becomes more severe. The SINR performance, in general, has an opposite behavior to that found in the power transfer performance, and it is shown that both the energy waveform and the single-tone waveform exhibit a significantly poorer SINR performance than the basic TR waveform and the MaxSINR waveform. Particularly, the performance difference is enlarged as L increases. This is because the waveforms designed from the power transfer maximization perspective aim at utilizing the multipath propagation effect to spread out the energy over the entire time duration, thereby raising the ISI level.

Fig. 4 shows the histograms of the power transfer performance for different waveforms in UWB channels with LOS and NLOS office environments. It is obvious from Fig. 4(a) that for the LOS setting, the power transfer performance of the optimal energy waveform is slightly better than that of the single-tone waveform in terms of the mean values in histograms. Both waveforms have better capability of recollecting the energy of all the possibly available multipaths at the receiver side than the other three waveforms. Again, the MaxSINR waveform has the worst power transfer performance among all the waveforms, since it is designed to maximize the received SINR from the information transmission perspective. A similar performance trend can be observed in Fig. 4(b) in the NLOS environments. However,

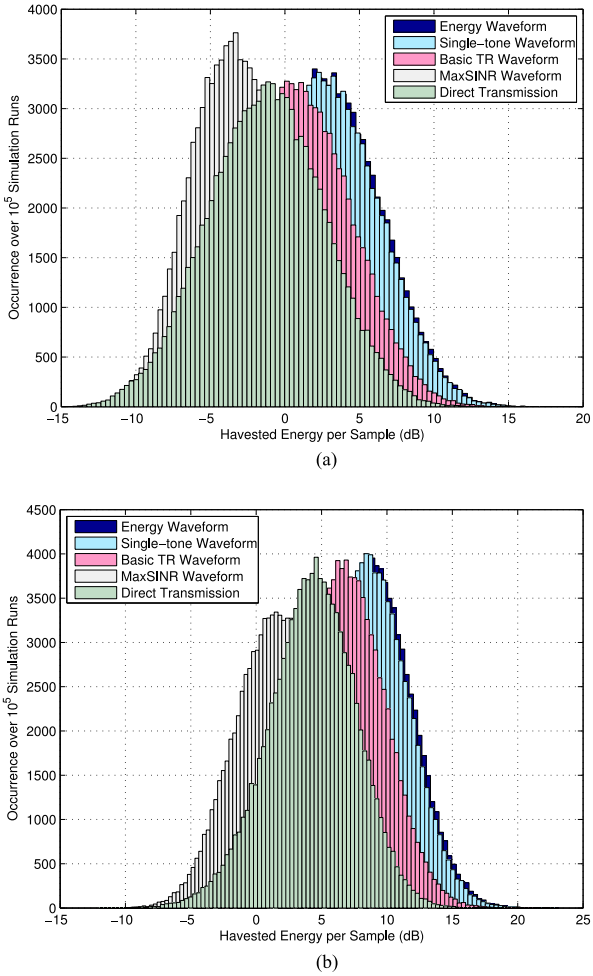

Fig. 4. Histograms of power transfer for different waveforms in UWB channels with LOS and NLOS environments. (a) UWB channel: office, LOS. (b) UWB channel: office, NLOS.

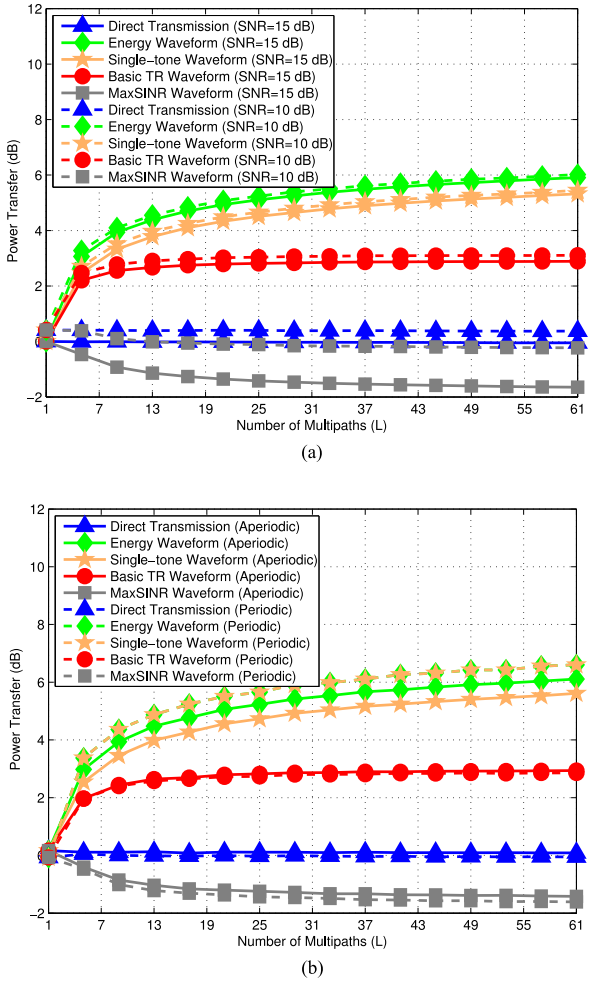

Fig. 5. Power transfer performance versus number of multipaths under UPD and TPD channel profiles for different waveforms. (a) UPD channel profile. (b) TPD channel profile with $\rho_0 = \frac{2}{L}$.

it is found that the harvested energy per sample in the NLOS environments is larger than that in the LOS environments.

Fig. 5(a) and (b) show the power transfer performance for different waveforms versus the number of multipaths under the UPD and TPD channel profiles, respectively. The parameter ρ_0 in the TPD channel profile is set as $\frac{2}{L}$. In Fig. 5(a), it is found that all waveforms, except for the MaxSINR waveform, follow a similar performance trend when SNR is decreased from 15 dB to 10 dB. This is because the design of the MaxSINR waveform makes a tradeoff between the ISI and noise effect, while the design of the other four waveforms is irrelevant to the noise power. In Fig. 5(b), it reveals that the performance of the two proposed waveforms with periodic signals is slightly better than that with aperiodic signals.

In Fig. 6, the power transfer performance of the single-tone waveform with periodic random transmitted signals is simulated and compared under the channel profiles, EPD, UPD and TPD. The parameter σ_T in the EPD channel profile could be 10 ns, 40 ns, and 80 ns, while the parameter ρ_0 in the TPD profile is given by $\frac{2}{L}$. For the EPD channel profile, it exhibits that the power transfer performance can be potentially improved as the delay spread σ_T increases, and the performance gets close to that in the UPD channel profile as σ_T is larger than 80 ns. It is possible to roughly infer the power transfer performance in the EPD channel profile by using the TPD channel profile and counting the effective number of multipaths. For example, let $\bar{L}$ be an effective number of dominant paths of a channel profile, which is defined as $\sum_{l=0}^{\bar{L}-1} \rho_l / \sum_{l=0}^{L-1} \rho_l \geq 99\%$, where $\bar{L}$ is a minimum integer satisfying the above inequality. Accordingly, for $L = 61$, the effect number of paths for the EPD channel profile with $\sigma_T = 10$ ns can be calculated as $\bar{L} = 6$. Interestingly, the attainable performance in this case is comparable to that in the TPD channel profile with $L = 6$.

The validity of the analytic power transfer gain for the single-tone waveform with periodic random transmitted signals in Theorem 5 and Theorem 6 is shown in Fig. 7. One can observe that for the UPD channel profile, the analytic result is exactly the same as the simulation result. On the other hand, for the TPD channel profile, the analytic result can serve as a good performance lower bound for the corresponding simulation result, and the bound becomes tight when the number of multipaths is sufficiently large. Hence, the provided analytic expressions are useful to predict the characteristic of the power transfer gains in multipath environments.

In Fig. 8, the analytical outage performances of the PW power transfer system and the MIMO power transfer system, derived in (24) and (25), are validated and compared by computer simulation, where the analytical results are plotted as solid curves, and the corresponding simulation results are marked by

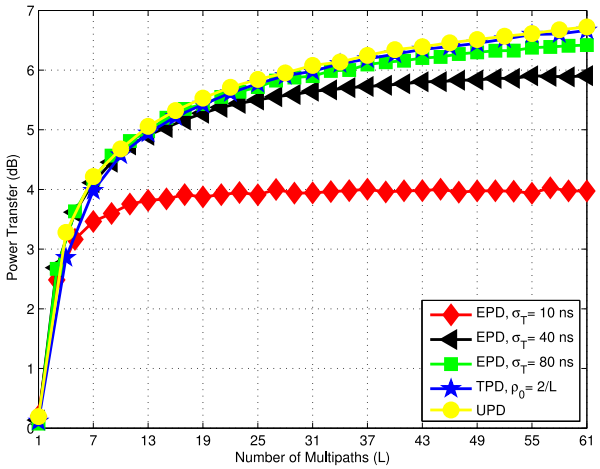

Fig. 6. Comparisons of power transfer performance of the single-tone waveform with periodic random transmitted signals under different channel profiles.

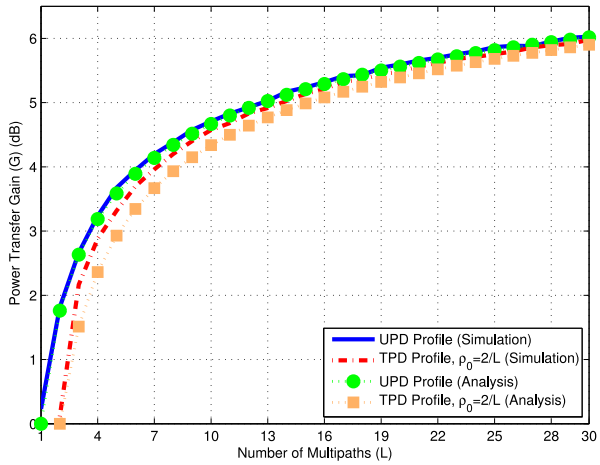

Fig. 7. Simulation and analytic results for the single-tone waveform with periodic random transmitted signals in UPD and TPD channel profiles.

different shapes. The subscript m of P_m on the y-axis could be "ST" or "MIMO." Without loss of generality, the transmit power is set as $P = 1$. One can find that there is a perfect match between the analytical and the simulation results. For the MIMO power transfer system, we can make the following observations. On one hand, the outage probability for $N_R = 1$ can be dramatically reduced by increasing the number of transmit antennas due to the transmit beamforming gain. On the other hand, for $N_T = 1$, the outage performance can be enhanced by an increased number of receive antennas. Actually, the outage performance of an MIMO system with $(N_T, N_R) = (N_1, N_2)$ is identical to that of a system with $(N_T, N_R) = (N_2, N_1)$, which can also be justified by using the outage probability formula in (24). For the PW power transfer system using the single-tone waveform, it is worth pointing out that the outage performance can be significantly enhanced when the number of resolvable multipaths is increased, while the improvement is less pronounced as L goes beyond 60. Table II summarizes the comparable setting values between $L^\star$ in the PW power transfer system and (N_T, N_R) in the conventional MIMO system for various outage probabilities P_{out} by using (26). We can find that the proposed PW power transfer system, which only requires a single antenna in implementation, can support a comparable performance as that using multi-antenna techniques. For instance, if the number of

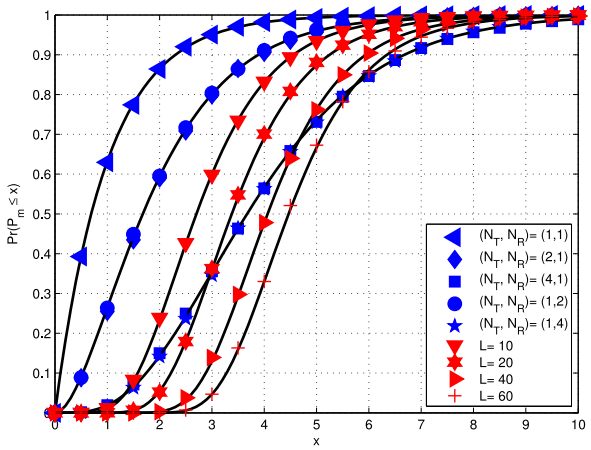

Fig. 8. Comparisons between the theoretical outage performance and simulation results of the MIMO power transfer system and the PW power transfer system ($P = 1$).

TABLE II
COMPARABLE SETTING VALUES BETWEEN PW POWER TRANSFER SYSTEMS AND CONVENTIONAL MIMO POWER TRANSFER SYSTEMS

$L^\star$		$N_T = 1$	$N_T = 2$	$N_T = 3$	$N_T = 4$
$N_R = 1$	$P_{out} = 0.7$	2	5	15	44
	$P_{out} = 0.8$	2	5	17	61
	$P_{out} = 0.9$	2	6	24	86
$N_R = 2$	$P_{out} = 0.7$	5	24	107	478
	$P_{out} = 0.8$	5	30	149	666
	$P_{out} = 0.9$	6	43	233	1153

resolvable multipaths is six, i.e., $L^\star = 6$, a PW power transfer system can achieve the same outage performance of $P_{\text{out}} = 0.9$ as 1×2 or 2×1 MIMO power transfer systems. When $L^\star$ is increased up to 24 or 43, which can be realized by enlarging the system bandwidth in practice, the proposed PW power transfer system is comparable to 3×1 or 2×2 MIMO systems at the outage probability of $P_{\text{out}} = 0.9$, respectively. It is worth pointing out that the performance of the PW power transfer system can also be enhanced by incorporating multiple antennas.

VII. Experimental Results and Discussions

The experimental study for the PW wireless power transfer systems is conducted to demonstrate the performance of the proposed PW methods and to explore the essential wireless power transfer characteristics in real wireless scattering environments, involving both the large-scale and small-scale fading effects. Our experiment platform is based on the transmitter/receiver developed by Origin Wireless Inc. The system is operated in the ISM band with the signal bandwidth 125 MHz, centered at the carrier frequency 5 GHz. The measurement is performed in the office environments in Origin Wireless Inc. A transmitter sends signals to a receiver by utilizing different kinds of waveforms in LOS and NLOS fashions, and the electromagnetic waves in the air are reflected by plentiful objectives in the surrounding areas.

The detailed floor plan and the layout of the experiments are shown in Fig. 9. The total space of the office environment in the experiment is around 882 m^2. For the layout of the experiment in the LOS testing environment, the transmitter and the receiver are randomly deployed in a rectangular shadowed area in an LOS manner, i.e., there is no blocking between them. The wireless power transfer distance is set from 1 meter to 6 meters with an increment of 1 meter, and the power transfer performance is

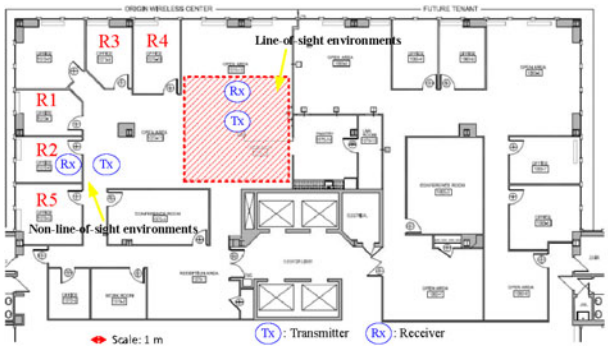

Fig. 9. Floor plan and the layout of the experiments in the LOS and NLOS testing environments. (Blue circles of Tx and Rx indicating the locations of the transmitter and the receiver, respectively).

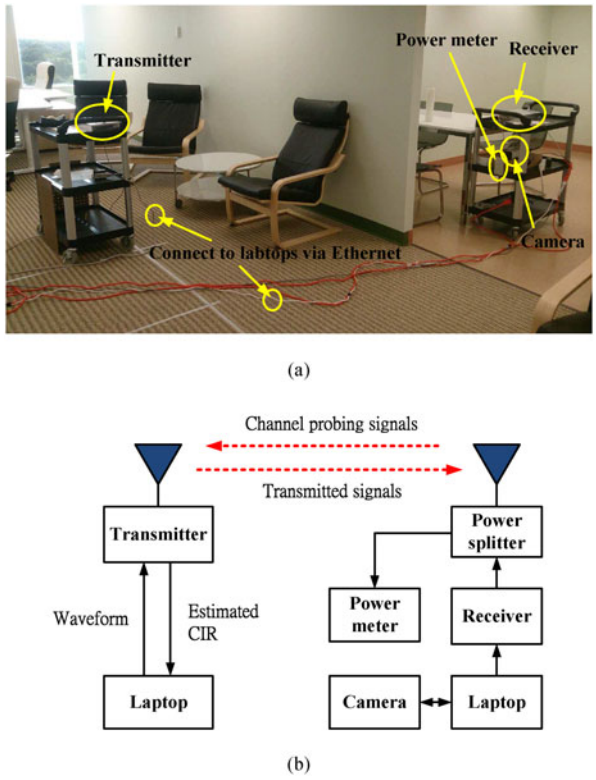

Fig. 10. Wireless power transfer measurement setup. (a) Photograph of the experiment setup for the transmitter and the receiver on two carts. (b) Detailed block diagram of the experiment setup.

measured at eight random locations (L1–L8) for each distance value. For the layout of the experiment in the NLOS testing environments, five office rooms (R1–R5) are considered, and the transmitter and the receiver are located outside and inside the room, respectively, just as an example sketched for the experiment in the room R2. For each room, three random locations (L1–L3) are adopted for the receiver in the experiments, and the distance between the transmitter and the receiver is set about 2 to 3 meters.

The photograph of the measurement setup and the detailed block diagram, including one transmitter, one receiver, one power splitter, one power meter, one camera and two labtops, are shown in Fig. 10(a) and (b), respectively. As mentioned above, the experiment of the PW wireless power transfer systems is mainly comprised of two phases. During the channel probing phase, the receiver sends channel probing signals to the transmitter for the purpose of CIR acquisition [36]. A channel estimator is applied to the received channel probing signals at the transmitter side for the estimation of the CIR [37]. During the power transfer phase, by assuming that the channel is reciprocal, the labtop connected to the transmitter first computes the digital waveforms according to the estimated CIR, and the transmitter then emits the signals shaped by the designed waveforms via an omni-directional antenna. In addition to the two PW methods, the other three waveforms developed primarily for information or focusing perspectives are also carried out in the experiments for performance comparisons. The maximum transmit power at the transmitter's radio frequency-front end is 20 dBm. At the receiver, a power meter CORNET ED85EXS, which is linked to the antenna via a power splitter ZX10-2-71+, is used to measure the received power at the radio frequency-front end, and a digital camera is set up to record the reported values on the power meter. The sensitivity range of the power meter is from -55 dBm up to 0 dBm. Finally, all the WiFi access points in the offices are turned off during the experiment.

Fig. 11 shows the PW wireless power transfer performance for different waveforms in the LOS and NLOS testing environments. For a fair comparison, the average transmit power of the different waveforms is normalized in such a way that the average transmit power is the same as that with the direct transmission waveform. The power transfer performance for the eight measured locations in the LOS setting at the distance of 2 meters is shown in Fig. 11(a). Due to the multipath effect, the power transfer performance, in terms of the observed power values on the power meter, varies for the different locations, even though the distance is merely two meters and the setting is LOS. As compared with the direct transmission waveform, the performance improvement achieved by the optimal energy waveform ranges from 4 dB to 8 dB. Taking an example, the improvement values at the locations L8 and L3 are respectively given as 4 dB and 8 dB, and one can observe from Fig. 12 that there are sufficient multipaths available even at such a short distance. Furthermore, the performances of the optimal energy and the single-tone waveforms are comparable, and the basic TR waveform is worse than the optimal energy waveform by about 2 dB $\sim$ 4 dB. Again, the power transfer performance of the MaxSINR waveform is worse in the experiment because it is designed from the information transfer viewpoint.

Fig. 11(b) demonstrates the average power transfer performance versus the distance in the LOS setting, for which the performance for each distance value is averaged over the eight random locations. We can find that for most of the cases, the average measured power value on the power meter is decreased when the distance becomes large due to the path loss effect. In addition, the optimal energy waveform is superior to the direct transmission waveform by about 6 dB in terms of the received power. Compared with the energy waveform, the single-tone waveform can achieve a near-optimal performance, but requires less computational complexity in implementation. It also exhibits that the performance of the TR waveform is about 3 dB worse than that of the energy waveform. Note that there is a jump at the distance of 5 m in terms of the performance of the received power. This is because in our testing environments, the wireless channels at the distance of 5 meters often appear to be more dispersed (i.e., more multipaths are collectable), as compared with the wireless channels at the distance of 3 or 4 meters. In general, the PW scheme can provide a larger performance gain, if the multipath effect is more severe. Hence, the average

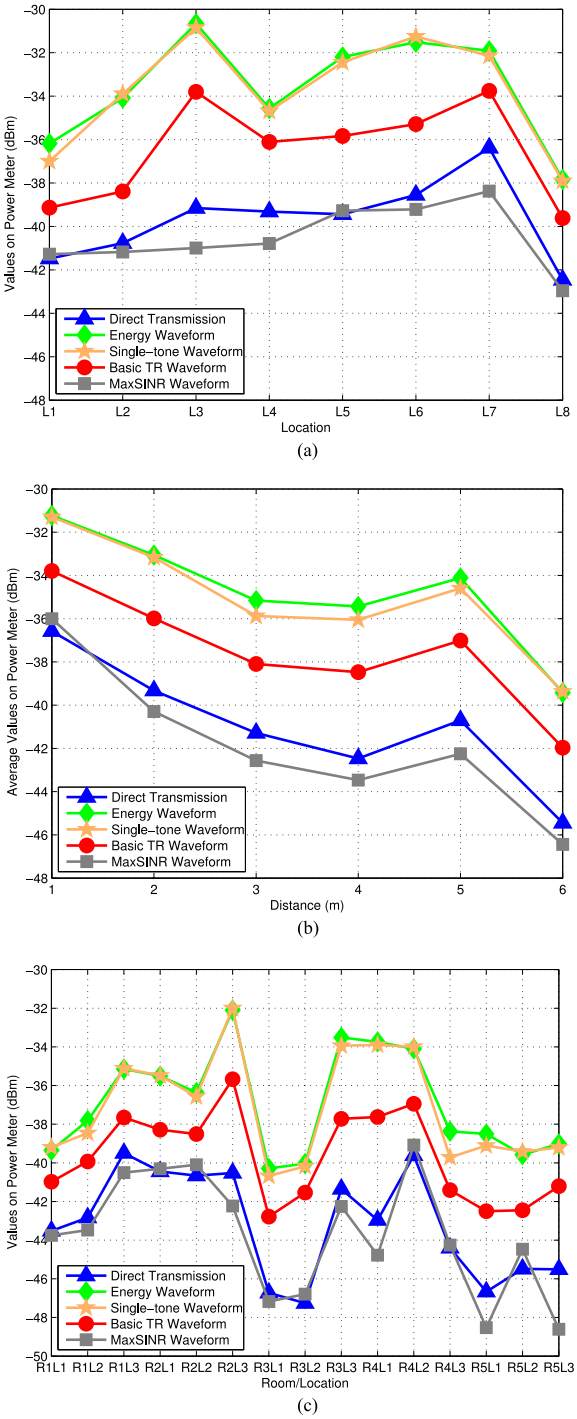

Fig. 11. PW wireless power transfer performance in LOS and NLOS environments. (a) Measurement results in the LOS environments for various locations at a distance of 2 meters. (b) Average measurement results in the LOS environments as a function of the separation between the transmitter and the receiver. (c) Measurement results in the NLOS environments for various rooms and locations.

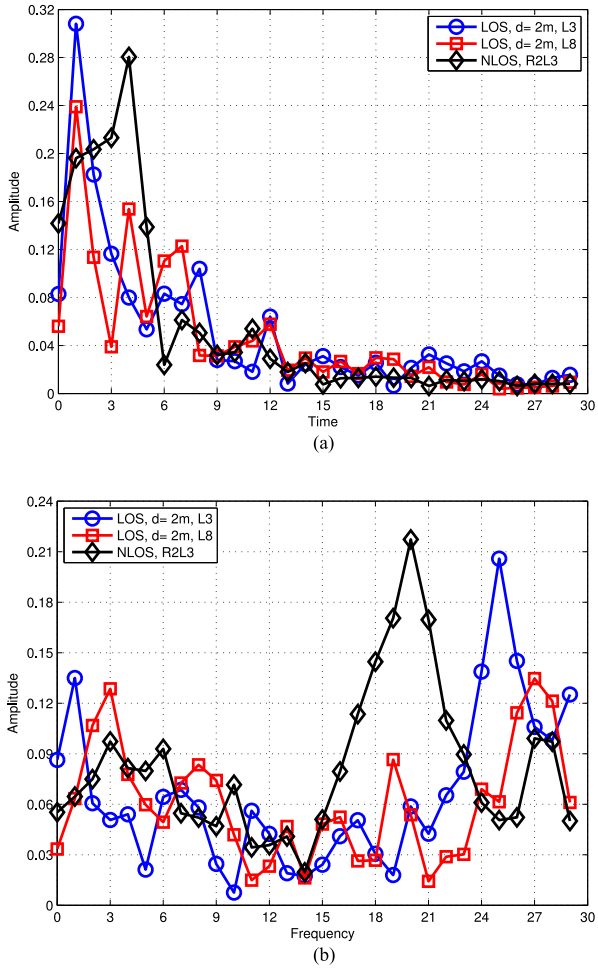

Fig. 12. Channel probing results in the LOS environments (d= 2 meters, and locations L3 and L8) and the NLOS environments (location R2L3). (a) The amplitude of CIRs versus time index. (b) The amplitude of CFRs versus frequency index.

received power value at the distance of 5 meters is larger than those measured at the distance of 3 or 4 meters, even though the radio waves may propagate over a relatively longer distance and suffer a larger path loss.

Fig. 11(c) shows the power measurement results for various rooms and locations in the NLOS testing environments. We can see that the performance gain of the optimal energy waveform over the direct transmission is larger than 6 dB for most of the locations, e.g., R2L3 and R3L1. It is worth pointing out that this performance gain in the NLOS environments is in general larger than that obtained in the LOS because the NLOS channel can provide a larger frequency selection diversity gain (see Fig. 12). Also, as compared with the direct transmission, the performance gain of using the optimal energy waveform (or the single-tone waveform) could be significantly different even in the same room but different locations; for example, the achievable performance gain is 9 dB at the location R4L1, whereas it is approximately given by 6 dB at the location R4L2. Overall, the single-tone waveform can still achieve a comparable (near-optimal) performance to the optimal energy waveform even in the NLOS environments. Finally, the performance gap between the energy waveform and the basic TR waveform ranges from 2 dB to 4 dB.

VIII. Conclusion

In this paper, a wireless power transfer system incorporating the PW technology was investigated to gather the multipath power by fully utilizing the multipath propagation effect. Two power transfer-oriented waveforms, energy waveform and single-tone waveform, were proposed with the goal of maximizing the average received signal power at the receiver. The

energy waveform is optimal in the sense of maximum power delivery, while the single-tone waveform is a low-complexity alternative at the expense of small performance degradation. In essence, the single-tone waveform could be just as good as the optimal one if a J-periodic condition for the transmitted signals is satisfied. The power transfer gain of the single-tone waveform over the direct transmission scheme was also theoretically analyzed under various channel power delay profiles. Besides, a comparable relationship between the proposed PW power transfer system and the conventional MIMO system is characterized through an outage performance analysis. It is conceived that the PW system can achieve a comparable performance to the MIMO system as long as the number of digitally resolvable multipaths at the transmitter is sufficiently large. As such, the PW technology is a practical and flexible solution to power transfer because the evolution of high-speed analog-to-digital converters (ADCs) allows the transmitter to digitally resolve as many as possible multipaths from wireless channels. On the contrary, the hardware implementation cost of the MIMO solution increases with the number of antennas, a key factor to the performance improvement. Extensive computer simulation was conducted to validate the analysis results, and it was further revealed that the proposed energy waveform and the single-tone waveform outperform other waveforms. Generally, the two proposed waveforms can provide a performance gain of about 6 dB over the direct transmission scheme. Real experiments were also implemented to justify the achievable performance gains. The results give a quantitative assessment of the impact of the number of resolvable multipaths on the power transfer performance.

APPENDIX A
PROOF OF THEOREM 1

Without loss of generality, we consider the zeroth segment of the received signal, i.e., $p = 0$. By applying (8) into (10) and using the uncorrelated property of $v[n]$, the power transfer maximization problem becomes

$$\mathbf{g}_E = \arg \max_{\|\mathbf{g}\|_2^2=1} \mathbf{g}^\dagger \left(\sum_{q=\lceil -1-(L-2)/D \rceil}^{\lfloor (L-1)/D \rfloor} \mathbf{H}_q^\dagger \mathbf{H}_q \right) \mathbf{g}. \quad \text{(A.1)}$$

Hence, the optimal energy waveform is given in (11). By substituting (9) into (A.1), we can also find that the optimal energy waveforms are the same for different values of D.

APPENDIX B
PROOF OF THEOREM 2

Since $L = J \cdot D$, we get $p - 1 - J + \lceil 2/D \rceil \le q \le p + J - 1$ in the summation of (8). As the signal is J-periodic, i.e., $v[n] = v[n + J]$, for any n, the received signal in (8) can be simplified as

$$\mathbf{y}_p = \begin{cases} \mathbf{H}_0 \mathbf{g} \cdot v[p] + \sum_{q=1}^{J-1} \left(\mathbf{H}_q + \mathbf{H}_{(q-J)} \right) \mathbf{g} \cdot v[p+q] \\ \qquad + \mathbf{z}_p, \quad D = 1; \\ \sum_{q=0}^{J-1} \left(\mathbf{H}_q + \mathbf{H}_{(q-J)} \right) \mathbf{g} \cdot v[p+q] + \mathbf{z}_p, \quad D \ge 2. \end{cases} \quad \text{(B.1)}$$

Let $\mathbf{C}$ be a circulant matrix of size $L \times L$, specified by the column vector of the CIR $\mathbf{h}$, and it is straightforward to verify from (9) that the matrix $\mathbf{C}$ and $\mathbf{H}_j$ has the following relationship:

$$\mathbf{C} = \begin{cases} \left[\mathbf{H}_{(J-1)}^T, \mathbf{H}_{(J-2)}^T, \ldots, \mathbf{H}_1^T, \mathbf{H}_0^T \right]^T \\ \quad + \left[\mathbf{H}_{-1}^T, \mathbf{H}_{-2}^T, \ldots, \mathbf{H}_{(1-J)}^T, \mathbf{O}_{1\times L}^T \right]^T, \quad D = 1; \\ \left[\mathbf{H}_{(J-1)}^T, \mathbf{H}_{(J-2)}^T, \ldots, \mathbf{H}_0^T \right]^T \\ \quad + \left[\mathbf{H}_{-1}^T, \mathbf{H}_{-2}^T, \ldots, \mathbf{H}_{-J}^T \right]^T, \quad D \ge 2. \end{cases} \quad \text{(B.2)}$$

By applying (B.1) and the uncorrelated property of $v[p+q]$, for $q = 0, \ldots, J-1$, the power transfer maximization problem in (10) becomes

$$\mathbf{g}_E = \arg \max_{\|\mathbf{g}\|_2^2=1} \mathbf{g}^\dagger \mathbf{C}^\dagger \mathbf{C} \mathbf{g}. \quad \text{(B.3)}$$

The circulant matrix $\mathbf{C}$ can be diagonalized as $\mathbf{F}\mathbf{C}\mathbf{F}^\dagger = \sqrt{L} \cdot \text{Diag}(\mathbf{F}\mathbf{h}) = \sqrt{L} \cdot \text{Diag}(\boldsymbol{\zeta})$. As a result, the optimal energy waveform must satisfy $\mathbf{F}\mathbf{g}_E = \mathbf{e}_{k_{\max}}$, where $\mathbf{e}_i$ is the i^{th} column of the identity matrix $\mathbf{I}_L$, for $i = 0, \ldots, L-1$. Hence, $\mathbf{g}_E = \mathbf{F}^\dagger \mathbf{e}_{k_{\max}}$ is exactly the same as the single-tone waveform $\mathbf{g}_{ST}$ given in (12).

APPENDIX C
PROOF OF THEOREM 3

Let $\mathbf{h}_I$ and $\mathbf{h}_Q$ be the real and imaginary parts of the CIR $\mathbf{h}$. In addition, we define $\mathbf{F}_I$ and $\mathbf{F}_Q$ as the real and imaginary parts of the DFT matrix $\mathbf{F}$. Since $\boldsymbol{\zeta} = \mathbf{F}\mathbf{h}$, its real and imaginary parts can be expanded as $\boldsymbol{\zeta}_I = \mathbf{F}_I \mathbf{h}_I - \mathbf{F}_Q \mathbf{h}_Q$ and $\boldsymbol{\zeta}_Q = \mathbf{F}_I \mathbf{h}_Q + \mathbf{F}_Q \mathbf{h}_I$, respectively. Therefore, it can be derived that

$$\begin{aligned} \mathbb{E}\left[\boldsymbol{\zeta}_I \boldsymbol{\zeta}_I^T\right] &= \mathbb{E}\left[\boldsymbol{\zeta}_Q \boldsymbol{\zeta}_Q^T\right] \triangleq \boldsymbol{\Sigma} \\ &= \frac{1}{2}\left(\mathbf{F}_I \text{Diag}(\boldsymbol{\rho}) \mathbf{F}_I^T + \mathbf{F}_Q \text{Diag}(\boldsymbol{\rho}) \mathbf{F}_Q^T \right); \quad \text{(C.1)} \end{aligned}$$

$$\mathbb{E}\left[\boldsymbol{\zeta}_I \boldsymbol{\zeta}_Q^T\right] = \mathbb{E}\left[\boldsymbol{\zeta}_Q \boldsymbol{\zeta}_I^T\right] = \mathbf{O}, \quad \text{(C.2)}$$

where the assumption of $\mathbb{E}[\mathbf{h}_I \mathbf{h}_I^T] = \mathbb{E}[\mathbf{h}_Q \mathbf{h}_Q^T] = \frac{1}{2}\text{Diag}(\boldsymbol{\rho})$ and $\mathbb{E}[\mathbf{h}_I \mathbf{h}_Q^T] = \mathbb{E}[\mathbf{h}_Q \mathbf{h}_I^T] = \mathbf{O}$ in (1) is applied. Due to (C.1) and (C.2), the characteristic function of $\boldsymbol{\varepsilon}$ has a form as shown in (17) [30], and the matrix $\boldsymbol{\Sigma}$ can be explicitly calculated in the following.

First, it is shown from (C.1) that the matrix $\boldsymbol{\Sigma}$ is circulant because the $(k,m)^{th}$ entry of $\boldsymbol{\Sigma}$ is given by

$$\Sigma[k,m] = \frac{1}{2L} \sum_{l=0}^{L-1} \rho_l \cos\left(-\frac{2\pi (k-m) l}{L} \right), \quad k, m = 0, \ldots, L-1. \quad \text{(C.3)}$$

Hence, by using $\mathbf{F}$, we can diagonalize the matrix into $\boldsymbol{\Sigma} = \mathbf{F}^{-1}\text{Diag}(\lambda)\mathbf{F}$, where the vector $\lambda = \sqrt{L}\mathbf{F}\mathbf{q}$, and $\mathbf{q} = \frac{1}{2L}\sum_{l=0}^{L-1} [\rho_l, \rho_l \cos(\frac{2\pi 1 l}{L}), \ldots, \rho_l \cos(\frac{2\pi (L-1) l}{L})]^T$ is the first column of the matrix $\boldsymbol{\Sigma}$, i.e., setting $m = 0$ in (C.3) [31]. We then rewrite $\mathbf{q}$ into a compact matrix form:

$$\mathbf{q} = \mathbf{M}\boldsymbol{\rho}, \quad \text{(C.4)}$$

where the matrix $\mathbf{M}$ is defined in (C.5) at the bottom of the next page. By applying (C.4) and (C.5), the $(k,m)^{th}$ entry of the

matrix $\tilde{\mathbf{M}} = \sqrt{L}\mathbf{F}\mathbf{M}$ can be computed as

$$\tilde{M}[k,m] = \begin{cases} \frac{1}{2}, & m=0; k=0; \\ \frac{1}{4}, & m \neq 0; k = L-m \neq m; \\ \frac{1}{2}, & m \neq 0; k = m = \frac{L}{2}; \\ 0, & \text{otherwise}, \end{cases} \tag{C.6}$$

if L is even, and

$$\tilde{M}[k,m] = \begin{cases} \frac{1}{2}, & m=0; k=0; \\ \frac{1}{4}, & m \neq 0; k = L-m \neq m; \\ 0, & \text{otherwise}, \end{cases} \tag{C.7}$$

if L is odd. Since $\lambda = \sqrt{L}\mathbf{F}\mathbf{q} = \tilde{\mathbf{M}}\boldsymbol{\rho}$, we finally get $\lambda_l = \frac{1}{4}(\rho_l + \rho_{((L-l)\%L)})$.

Appendix D
Proof of Theorem 4

The cumulative distribution function (CDF) of $\boldsymbol{\varepsilon}$ can be expressed in terms of $\Psi_{\boldsymbol{\varepsilon}}(j\boldsymbol{\omega})$ as follows [32]:

$$F_{\boldsymbol{\varepsilon}}(\mathbf{x}) = \frac{1}{(2\pi)^L}\int_{-\infty}^{\infty}\cdots\int_{-\infty}^{\infty}\Psi_{\boldsymbol{\varepsilon}}(j\boldsymbol{\omega}) \times \prod_{l=0}^{L-1}\left(\frac{1-e^{-j\omega_l x_l}}{j\omega_l}\right)d\omega_0\cdots d\omega_{L-1}, \tag{D.1}$$

where $\mathbf{x} = [x_0,\ldots,x_{L-1}]^T$. Let $\varepsilon_{\max} = \max_k \varepsilon_k$. The CDF of $\varepsilon_{\max}$ is then obtained by letting $x_0 = \cdots = x_{L-1} = x$ in (D.1), and we have

$$F_{\varepsilon_{\max}}(x) = \frac{1}{(2\pi)^L}\int_{-\infty}^{\infty}\cdots\int_{-\infty}^{\infty}\Psi_{\boldsymbol{\varepsilon}}(j\boldsymbol{\omega}) \times \prod_{l=0}^{L-1}\left(\frac{1-e^{-j\omega_l x}}{j\omega_l}\right)d\omega_0\cdots d\omega_{L-1}. \tag{D.2}$$

Since $\varepsilon_{\max}$ is a non-negative random variable, the mean of $\varepsilon_{\max}$ can be directly computed through its CDF, which follows essentially from integration by parts:

$$\mathbb{E}[\varepsilon_{\max}] = \int_0^{\infty}(1-F_{\varepsilon_{\max}}(x))\,dx. \tag{D.3}$$

From (16), (D.2) and (D.3), the power transfer gain is finally derived in (18).

Appendix E
Proof of Theorem 5

For the UPD channel profile, we have $\rho_l = \frac{1}{L}$, for $l = 0,\ldots,L-1$. From (17) in Theorem 3, it is then shown that $\lambda_l = \frac{1}{2L}$ and the characteristic function is reduced to

$$\Psi_{\boldsymbol{\varepsilon}}(j\boldsymbol{\omega}) = \left(\det\left(\mathbf{I}_L - j\frac{1}{L}\cdot\mathrm{Diag}(\boldsymbol{\omega})\,\mathbf{F}^{-1}\mathbf{F}\right)\right)^{-1} = \prod_{l=0}^{L-1}\frac{L}{L-j\omega_l}, \tag{E.1}$$

where $\mathbf{F}^{-1}\mathbf{F} = \mathbf{I}_L$ is applied in the second equality. Moreover, considering an exponential random variable x with the probability density function $\mu e^{-\mu x}$, for $\mu > 0$, its characteristic function $\Psi_X(j\omega) = \frac{\mu}{\mu - j\omega}$ and the corresponding CDF $F_X(x) = 1 - e^{-\mu x}$ have the following relationship:

$$F_X(x) = \frac{1}{2\pi}\int_{-\infty}^{\infty}\Psi_X(j\omega)\frac{1-e^{-j\omega x}}{j\omega}d\omega = \frac{1}{2\pi}\int_{-\infty}^{\infty}\frac{\mu}{\mu-j\omega}\times\frac{1-e^{-j\omega x}}{j\omega}d\omega = 1-e^{-\mu x}. \tag{E.2}$$

By applying (E.2) into (18), the power transfer gain can be derived as

$$\begin{aligned} G &= L\int_0^{\infty}\left(1-\frac{1}{(2\pi)^L}\int_{-\infty}^{\infty}\cdots\int_{-\infty}^{\infty}\prod_{l=0}^{L-1}\left(\frac{L}{L-j\omega_l}\cdot\frac{1-e^{-j\omega_l x}}{j\omega_l}\right)d\omega_0\cdots d\omega_{L-1}\right)dx \\ &= L\int_0^{\infty}\left(1-\frac{1}{(2\pi)^{L-1}}\int_{-\infty}^{\infty}\cdots\int_{-\infty}^{\infty}\prod_{l=1}^{L-1}\left(\frac{L}{L-j\omega_l}\cdot\frac{1-e^{-j\omega_l x}}{j\omega_l}\right)\cdot\left(\frac{1}{2\pi}\int_{-\infty}^{\infty}\frac{L}{L-j\omega_0}\cdot\frac{1-e^{-j\omega_0 x}}{j\omega_0}d\omega_0\right)\right. \\ &\quad \left.\times\, d\omega_1\cdots d\omega_{L-1}\right)dx \\ &= L\int_0^{\infty}\left(1-\left(1-e^{-Lx}\right)^L\right)dx. \end{aligned} \tag{E.3}$$

Using the binomial expansion, we can get

$$\left(1-e^{-Lx}\right)^L = \sum_{n=0}^{L}\binom{L}{n}(-1)^n e^{-nLx}. \tag{E.4}$$

$$\mathbf{M} = \frac{1}{4L}\begin{bmatrix} 2 & 2 & \cdots & 2 \\ 2 & e^{j2\pi 1\cdot 1/L} + e^{j2\pi 1\cdot(L-1)/L} & \cdots & e^{j2\pi 1\cdot(L-1)/L} + e^{j2\pi 1\cdot 1/L} \\ \vdots & \vdots & \ddots & \vdots \\ 2 & e^{j2\pi(L-1)\cdot 1/L} + e^{j2\pi(L-1)\cdot(L-1)/L} & \cdots & e^{j2\pi(L-1)\cdot(L-1)/L} + e^{j2\pi(L-1)\cdot 1/L} \end{bmatrix}. \tag{C.5}$$

From (E.3) and (E.4), it therefore implies that

$$G = L\sum_{n=1}^{L}\binom{L}{n}(-1)^{n+1}\int_0^\infty e^{-nLx}dx = \sum_{n=1}^{L}\binom{L}{n}(-1)^{n+1}\frac{1}{n}, \tag{E.5}$$

where $\binom{L}{n} = \frac{L!}{n!(L-n)!}$ is a binomial coefficient, and $(\cdot)!$ is a factorial function. To further inspect the impact of the number of multipaths on the performance, we denote the power transfer gain as a function of L, given by $G(L)$. From (E.5), it can be verified that

$$G(L) - G(L-1) = -\frac{1}{L}\left(\sum_{n=0}^{L}\frac{L!}{n!(L-n)!}(-1)^n - 1\right). \tag{E.6}$$

From the binomial expansion, it yields $\sum_{n=0}^{L}\frac{L!}{n!(L-n)!}(-1)^n = (1+(-1))^L = 0$. Thus, it can be shown that $G(L) - G(L-1) = \frac{1}{L} \geq 0$. Finally, since $G(1) = 1$ according to (E.5), it is straightforward to get (19).

Appendix F
Proof of Theorem 6

The main idea of the proof is to decompose the zeroth channel path of (1), h_0, into two independent random variables:

$$h_0 = h_{0,1} + h_{0,2}, \tag{F.1}$$

where $h_{0,1}$ and $h_{0,2}$ are zero-mean complex Gaussian random variables with variance $\frac{1-\rho_0}{L-1}$ and $\frac{L\rho_0-1}{L-1}$, respectively. By utilizing (16), the power transfer gain is given as

$$G = L\cdot\mathbb{E}\left[\max_k\left|\frac{1}{\sqrt{L}}h_{0,2} + \tilde{H}[k]\right|^2\right], \tag{F.2}$$

where $\tilde{H}[k] = \frac{1}{\sqrt{L}}(h_{0,1} + \sum_{l=1}^{L-1}h_l e^{-j2\pi kl/L})$. Let $\tilde{k}_{\max} = \arg\max_k |\tilde{H}[k]|^2$. Then, a lower bound can be derived as

$$G \geq L\cdot\mathbb{E}\left[\left|\frac{1}{\sqrt{L}}h_{0,2} + \tilde{H}\left[\tilde{k}_{\max}\right]\right|^2\right]. \tag{F.3}$$

Since $h_{0,2}$ is independent of $\tilde{H}[k]$, we have

$$G \geq \mathbb{E}\left[|h_{0,2}|^2\right] + L\cdot\mathbb{E}\left[\left|\tilde{H}\left[\tilde{k}_{\max}\right]\right|^2\right] = \frac{L\rho_0 - 1}{L-1} + L\cdot\mathbb{E}\left[\left|\tilde{H}\left[\tilde{k}_{\max}\right]\right|^2\right]. \tag{F.4}$$

The remaining problem is to compute the expectation value of $|\tilde{H}[\tilde{k}_{\max}]|^2$. Let us define $\tilde{\boldsymbol{\varepsilon}} = [\tilde{\varepsilon}_0, \ldots, \tilde{\varepsilon}_{L-1}]^T$, where $\tilde{\varepsilon}_k = |\tilde{H}[k]|^2$. Similar to the derivation in (E.1)–(E.5), the characteristic function for $\tilde{\boldsymbol{\varepsilon}}$ can be expressed as

$$\Psi_{\tilde{\boldsymbol{\varepsilon}}}(j\boldsymbol{\omega}) = \left(\det\left(\mathbf{I}_L - j\frac{1-\rho_0}{L-1}\cdot\mathrm{Diag}(\boldsymbol{\omega})\right)\right)^{-1} = \prod_{l=0}^{L-1}\frac{L-1}{L-1-j(1-\rho_0)\omega_l}. \tag{F.5}$$

Furthermore, we get

$$\mathbb{E}\left[\left|\tilde{H}\left[\tilde{k}_{\max}\right]\right|^2\right] = \int_0^\infty\left(1-\left(1-e^{-\frac{L-1}{1-\rho_0}x}\right)^L\right)dx = \frac{1-\rho_0}{L-1}\sum_{n=1}^{L}\binom{L}{n}(-1)^{n+1}\frac{1}{n}. \tag{F.6}$$

By combining (F.4) with (F.6), the result is finally proved.

References

[1] A. Luigi, I. Antonio, and M. Giacomo, "The Internet of things: A survey," *Comput. Netw.*, vol. 54, no. 15, pp. 2787–2805, Oct. 2010.

[2] C. Han *et al.*, "Green radio: Radio techniques to enable energy-efficient networks," *IEEE Commun. Mag.*, vol. 49, no. 6, pp. 46–54, Jun. 2011.

[3] S. Sudevalayam and P. Kulkarni, "Energy harvesting sensor nodes: Survey and implications," *IEEE Commun. Surveys Tuts.*, vol. 13, no. 3, pp. 443–461, 3rd Quart., 2011.

[4] M.-L. Ku, W. Li, Y. Chen, and K. J. Ray Liu, "Advances in energy harvesting communications: Past, present, and future challenges," *IEEE Commun. Surveys Tuts.*, vol. 18, no. 2, pp. 1384–1412, 2nd Quart., 2016.

[5] M.-L. Ku, Y. Chen, and K. J. R. Liu, "Data-driven stochastic models and policies for energy harvesting sensor communications," *IEEE J. Sel. Areas Commun.*, vol. 33, no. 8, pp. 1505–1520, Aug. 2015.

[6] R. J. M. Vullers, R. V. Schaijk, H. J. Visser, J. Penders, and C. V. Hoof, "Energy harvesting for autonomous wireless sensor networks," *IEEE Solid-State Circuits Mag.*, vol. 2, no. 2, pp. 29–38, Spring 2010.

[7] X. Lu, P. Wang, D. Niyato, D. Kim, and Z. Han, "Wireless charging technologies: Fundamentals, standards, and network applications," *IEEE Commun. Surveys Tuts.*, vol. 18, no. 2, pp. 1413–1452, 2nd Quart., 2016.

[8] N. B. Carvalho *et al.*, "Wireless power transmission: R&D activities within Europe," *IEEE Trans. Microw. Theory Techn.*, vol. 62, no. 4, pp. 1031–1045, Apr. 2014.

[9] S. Kim *et al.*, "Ambient RF energy-harvesting technologies for self-sustainable standalone wireless sensor platforms," *Proc. IEEE*, vol. 102, no. 11, pp. 1649–1666, Nov. 2014.

[10] X. Chen, Z. Zhang, H.-H. Chen, and H. Zhang, "Enhancing wireless information and power transfer by exploiting multi-antenna techniques," *IEEE Commun. Mag.*, vol. 53, no. 4, pp. 133–141, Apr. 2015.

[11] K. Huang and V. K. N. Lau, "Enabling wireless power transfer in cellular networks: Architecture, modeling and deployment," *IEEE Trans. Wireless Commun.*, vol. 13, no. 2, pp. 902–912, Feb. 2014.

[12] L. Liu, R. Zhang, and K.-C. Chua, "Multi-antenna wireless powered communication with energy beamforming," *IEEE Trans. Commun.*, vol. 62, no. 12, pp. 4349–4361, Dec. 2014.

[13] G. Yang, C. K. Ho, and Y. L. Guan, "Multi-antenna wireless energy transfer for backscatter communication systems," *IEEE J. Sel. Areas Commun.*, vol. 33, no. 12, pp. 2974–2987, Dec. 2015.

[14] Z. Fang, X. Yuan, and X. Wang, "Distributed energy beamforming for simultaneous wireless information and power transfer in the two-way relay channel," *IEEE Trans. Signal Process. Lett.*, vol. 22, no. 6, pp. 656–660, Jun. 2015.

[15] Y. Zeng and R. Zhang, "Optimized training design for wireless energy transfer," *IEEE Trans. Commun.*, vol. 63, no. 2, pp. 536–550, Feb. 2015.

[16] J. Xu and R. Zhang, "Energy beamforming with one-bit feedback," *IEEE Trans. Signal Process.*, vol. 62, no. 20, pp. 5370–5381, Oct. 2014.

[17] S. Kashyap, E. Bjornson, and E. G. Larsson, "Can wireless power transfer benefit from large transmitter arrays?" in *Proc. IEEE Wireless Power Transfer Conf.*, 2015, pp. 1–3.

[18] X. Chen, X. Wang, and X. Chen, "Energy-efficient optimization for wireless information and power transfer in large-scale MIMO systems employing energy beamforming," *IEEE Wireless Commun. Lett.*, vol. 2, no. 6, pp. 667–670, Dec. 2013.

[19] G. Yang, C. Keong Ho, R. Zhang, and Y. L. Guan, "Throughput optimization for massive MIMO systems powered by wireless energy transfer," *IEEE J. Sel. Areas Commun.*, vol. 33, no. 8, pp. 1640–1650, Aug. 2015.
[20] B. Wang, Y. Wu, F. Han, Y.-H. Yang, and K. J. R. Liu, "Green wireless communications: A time-reversal paradigm," *IEEE J. Sel. Areas Commun.*, vol. 29, no. 8, pp. 1698–1710, Sep. 2011.
[21] Y. Chen, Y.-H. Yang, F. Han, and K. J. R. Liu, "Time-reversal wideband communications," *IEEE Trans. Signal Process. Lett.*, vol. 20, no. 12, pp. 1219–1222, Dec. 2013.
[22] Y. Chen, B. Wang, Y. Han, H.-Q. Lai, Z. Safar, and K. J. Ray Liu, "Why time-reversal for future 5G wireless?," *IEEE Signal Process. Mag.*, vol. 33, no. 2, pp. 17–26, Mar. 2016.
[23] Y.-H. Yang, B. Wang, W. S. Lin, and K. J. R. Liu, "Near-optimal waveform design for sum rate optimization in time-reversal multiuser downlink systems," *IEEE Trans. Wireless Commun.*, vol. 12, no. 1, pp. 346–357, Jan. 2013.
[24] G. Yang, C. K. Ho, R. Zhang, and Y. L. Guan, "Throughput optimization for massive MIMO systems powered by wireless energy transfer," *IEEE J. Sel. Areas Commun.*, vol. 33, no. 8, pp. 1640–1650, Aug. 2015.
[25] S. Luo, J. Xu, T. J. Lim, and R. Zhang, "Capacity region of MISO broadcast channel for simultaneous wireless information and power transfer," *IEEE Trans. Commun.*, vol. 62, no. 10, pp. 3856–3868, Oct. 2015.
[26] X. Zhou, C. K. Ho, and R. Zhang, "Wireless power meets energy harvesting: A joint energy allocation approach in OFDM-based system," *IEEE Trans. Wireless Commun.*, vol. 15, no. 5, pp. 3481–3491, May 2016.
[27] X. Zhou, R. Zhang, and C. K. Ho, "Wireless information and power transfer in multiuser OFDM systems," *IEEE Trans. Wireless Commun.*, vol. 13, no. 4, pp. 2282–2294, Apr. 2014.
[28] Y. Zeng and R. Zhang, "Optimized training for net energy maximization in multi-antenna wireless energy transfer over frequency-selective channel," *IEEE Trans. Commun.*, vol. 63, no. 6, pp. 2360–2373, Jun. 2015.
[29] A. A. M. Saleh and R. A. Valenzuela, "A statistical model for indoor multipath propagation," *IEEE J. Sel. Areas Commun.*, vol. 5, no. 2, pp. 128–137, Feb. 1987.
[30] R. K. Mallik, "On multivariate Rayleigh and exponential distributions," *IEEE Trans. Inform. Theory*, vol. 49, no. 6, pp. 1499–1515, Jun. 2003.
[31] R. A. Horn and C. R. Johnson, *Matrix Analysis*. New York, NY, USA: Cambridge Univ. Press, 1985.
[32] Q. T. Zhang and H. G. Lu, "A general analytical approach to multi-branch selection combining over various spatially correlated fading channels," *IEEE Trans. Commun.*, vol. 50, no. 7, pp. 1066–1073, Jul. 2002.
[33] N. Kong and L. B. Milstein, "Average SNR of a generalized diversity selection combining scheme," *IEEE Trans. Commun. Lett.*, vol. 3, no. 3, pp. 57–59, Mar. 1999.
[34] M. Kang and M.-S. Alouini, "Largest eigenvalue of complex Wishart matrices and performance analysis of MIMO MRC systems," *IEEE J. Sel. Areas Commun.*, vol. 21, no. 3, pp. 418–426, Apr. 2003.
[35] M. Abramowitz and I. A. Stegun, *Handbook of Mathematical Functions With Formulas, Graphs, and Mathematical Tables*, 9th ed. New York, NY, USA: Dover, 1970.
[36] S. Budišin, "Golay complementary sequences are superior to PN sequences," in *Proc. IEEE Int. Conf. Syst. Eng.*, 1992, pp. 101–104.
[37] B. M. Popovic, "Efficient Golay correlator," *Electron. Lett.*, vol. 35, no. 17, pp. 1427–1428, Aug. 1999.

Meng-Lin Ku (M'11) received the B.S., M.S., and Ph.D. degrees from the National Chiao Tung University, Hsinchu, Taiwan, in 2002, 2003, and 2009, respectively, all in communication engineering. Between 2009 and 2010, he was a Postdoctoral Research Fellow with Prof. L.-C. Wang in the Department of Electrical and Computer Engineering, National Chiao Tung University, and with Prof. V. Tarokh in the School of Engineering and Applied Sciences, Harvard University. In August 2010, he became a Faculty Member of the Department of Communication Engineering, National Central University, Jung-li, Taiwan, where he is currently an Associate Professor. During the summer of 2013, he was a Visiting Scholar in the Signals and Information Group of Prof. K. J. Ray Liu at the University of Maryland. His research interests include the areas of green communications, cognitive radios, and optimization of radio access. He received the Best Counseling Award in 2012 and the University-Level Best Teaching Award in 2014, 2015, and 2016 at National Central University. He also received the Exploration Research Award of the Pan Wen Yuan Foundation, Taiwan, in 2013.

Yi Han received the B.S. degree in electrical engineering (highest honor) from Zhejiang University, Hangzhou, China, in 2011, and the Ph.D. degree from the Department of Electrical and Computer Engineering, University of Maryland, College Park, MD, USA. His research interests include wireless communication and signal processing. He received Class A Scholarship from Chu Kochen Honors College, Zhejiang University, in 2008, and also the Best Student Paper Award at the IEEE International Conference on Acoustics, Speech, and Signal Processing in 2016.

Hung-Quoc Lai (M'11) received the B.S. (*cum laude*), M.S., and Ph.D. degrees from the University of Maryland, College Park, MD, USA, in 2004, 2006, and 2011, respectively, all in electrical engineering.

His research interests include ultrawideband communications, cooperative communications, and networking. He is a Gates Millennium Scholar. He received University-Level Distinguished Teaching Assistant Award from the University of Maryland and the 2005 George Corcoran Award from the Department of Electrical and Computer Engineering, University of Maryland.

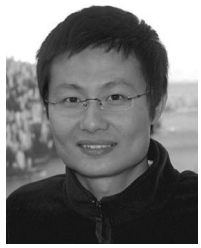

Yan Chen (SM'14) received the Bachelor's degree from the University of Science and Technology of China, Hefei, China, in 2004, the M.Phil. degree from Hong Kong University of Science and Technology, Hong Kong, in 2007, and the Ph.D. degree from the University of Maryland, College Park, MD, USA, in 2011.

Being a Founding Member, he joined Origin Wireless, Inc., as a Principal Technologist in 2013. He is currently a Professor with the University of Electronic Science and Technology of China, Chengdu, China. His research interests include multimedia, signal processing, game theory, and wireless communications. He received multiple honors and awards, including the Best Student Paper Award at the IEEE International Conference on Acoustics, Speech, and Signal Processing in 2016, the Best Paper Award at the IEEE International Conference on Global Communications in 2013, the Future Faculty Fellowship and Distinguished Dissertation Fellowship Honorable Mention from the Department of Electrical and Computer Engineering in 2010 and 2011, the Finalist of the Dean's Doctoral Research Award from the A. James Clark School of Engineering, the University of Maryland in 2011, and the Chinese Government Award for outstanding students abroad in 2010.

K. J. Ray Liu (F'03) was named in 2007 a Distinguished Scholar Teacher of the University of Maryland, College Park, MD, USA, where he is a Christine Kim Eminent Professor of information technology. He leads the Maryland Signals and Information Group conducting research encompassing broad areas of information and communications technology with recent focus on future wireless technologies, network science, and information forensics and security.

He is a Member of the IEEE Board of Director. He was the President of the IEEE Signal Processing Society, where he has served as the Vice President—Publications and the Board of Governor. He has also served as the Editor-in-Chief of the IEEE SIGNAL PROCESSING MAGAZINE.

He received the 2016 IEEE Leon K. Kirchmayer Technical Field Award on graduate teaching and mentoring, the IEEE Signal Processing Society 2014 Society Award, and the IEEE Signal Processing Society 2009 Technical Achievement Award. Recognized by Thomson Reuters as a highly cited researcher, he is a Fellow of the AAAS.

He also received teaching and research recognitions from the University of Maryland including University-Level Invention of the Year Award; and College-Level Poole and Kent Senior Faculty Teaching Award, Outstanding Faculty Research Award, and Outstanding Faculty Service Award, all from A. James Clark School of Engineering.